NOAA Technical Report ERL 337-APCL 36

U.S. DEPARTMENT OF COMMERCE
NATIONAL OCEANIC AND ATMOSPHERIC ADMINISTRATION
Environmental Research Laboratories

Physical and Chemical Properties of AgI Aerosols Formed at Simulated Airborne Conditions

F. P. PARUNGO
R. F. PUESCHEL
B. T. PATTEN
D. EYRE

BOULDER, COLO.
SEPTEMBER 1975

U.S. DEPARTMENT OF COMMERCE
Rogers C. B. Morton, Secretary

NATIONAL OCEANIC AND ATMOSPHERIC ADMINISTRATION
Robert M. White, Administrator
ENVIRONMENTAL RESEARCH LABORATORIES
Wilmot N. Hess, Director

NOAA TECHNICAL REPORT ERL 337-APCL 36

Physical and Chemical Properties of AgI Aerosols Formed at Simulated Airborne Conditions

F. P. PARUNGO
R. F. PUESCHEL
B. T. PATTEN
D. EYRE

BOULDER, COLO.
September 1975

For sale by the Superintendent of Documents, U. S. Government Printing Office, Washington, D. C. 20402

NOTICE

The Environmental Research Laboratories do not approve, recommend, or endorse any proprietary product or proprietary material mentioned in this publication. No reference shall be made to the Environmental Research Laboratories or to this publication furnished by the Environmental Research Laboratories in any advertising or sales promotion which would indicate or imply that the Environmental Research Laboratories approve, recommend, or endorse any proprietary product or proprietary material mentioned herein, or which has as its purpose an intent to cause directly or indirectly the advertised product to be used or purchased because of this Environmental Research Laboratories publication.

CONTENTS

ABSTRACT

AgI cloud-seeding nuclei were produced in a wind tunnel by both a flame generator and pyrotechnic at simulated aircraft speeds (150 to 200 mph). These aerosols were collected with isokenetic and anisokinetic samplers. By using electron-microscope combined with X-ray energy spectrometer, we determined the particles' size, shape, chmical composition, photostability, and hygroscopicity. We also studied the relationship between these properties and the AgI aerosols' effectiveness as sublimation, condensation-freezing, and contact nuclei. All the aerosols' properties depend on the generating techniques, the additives mixed with AgI before combustion, and the quenching rate of the exhaust plume.

From our study of the existing aerosol-generating methods, we developed a new method: combusting solid AgI in a flame generator. We found the aerosol's size distribution, chemical arrangement, and physical properties can be controlled by mixing another salt with the solid AgI; this promotes heterogeneous nucleation or modifies the surface characteristics during the vapor-to-particle transition. This new method has the potential of delivering an AgI aerosol having these properties required for ice nuclei in a particular cloud seeding operation.

PHYSICAL AND CHEMICAL PROPERTIES OF AgI AEROSOLS FORMED AT SIMULATED AIRBORNE CONDITIONS

F. P. Parungo, R. F. Pueschel, B. T. Patten[1], and D. Eyre

1. INTRODUCTION

Since the beginning of cloud seeding experiments, the importance of studying seeding materials has been recognized. To accurately evaluate this effect, we must know the physical and chemical properties of the seeding aerosol. Vonnegut (1949) and Peña and Caimi (1967) measured the size distribution and chemical composition of silver iodide (AgI) particles produced by a ground generator. However, airborne seeding techniques have recently replaced ground generators, because they are faster and more accurate on their delivery of AgI aerosols into selected clouds. Consequently, Mossop and Tuck-Lee (1968) analyzed the AgI particles produced by an airborne generator in a wind tunnel, but the airflow used was slower than an aircraft's speed, and their samples were collected at anisokinetic conditions. Since the aerosol's size and properties critically depend on the quenching rate of the hot gases after combustion as well as the sampling technique, these measurements would not necessarily reflect the AgI aerosol formed and collected during an actual airborne seeding experiment.

To accurately determine the chemical and physical properties of the AgI aerosol produced by airborne techniques, we conducted three sets of experiments in a wind tunnel at simulated airborne conditions.

For our experiments, we chose the Federal Aviation Administration (FAA) wind tunnel at Atlantic City, New Jersey (National Aviation Facilities Experimental Center). It is an open-circuit, induction-type tunnel 50 m long with a 2 m diameter test section (figs. 1 and 2, table 1). Two Pratt and Whitney J-57-F19W turbojet engines, supported on each side of the tunnel at midway, can simulate an air speed up to 650 mph (289 m sec^{-1}). All our experiments were conducted in the area forward of the entrances of the engine exhaust gases; this avoided the exhaust aerosols interfering with the samples. Three different aerosol generating methods were tested under the following conditions.

---

[1] Employed by the Research Faciliites Center of Office of Weather Modification.

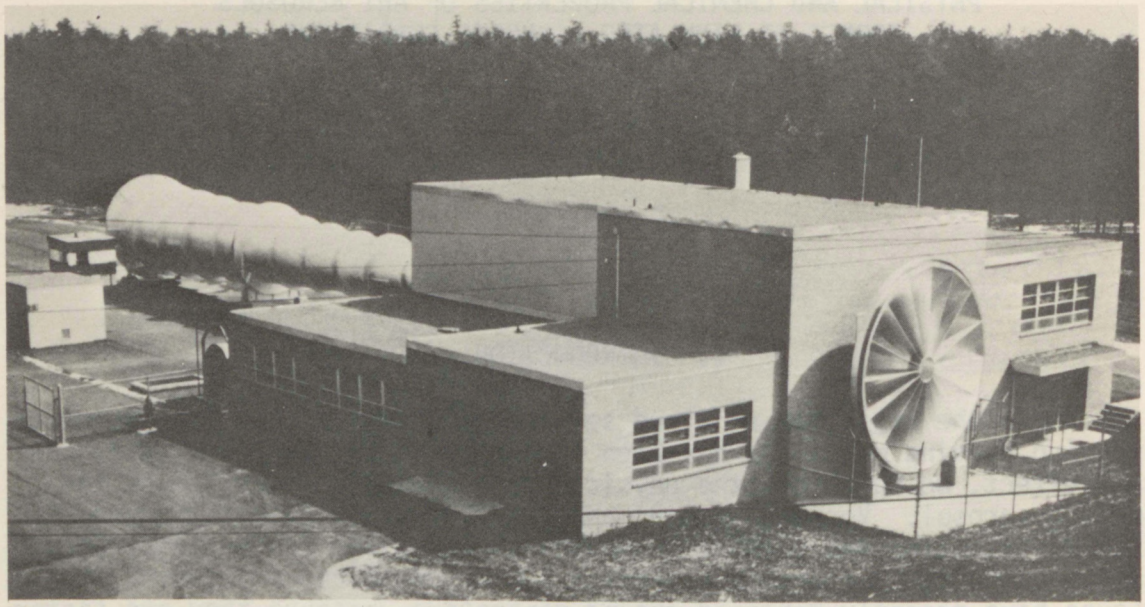

Figure 1. Wind tunnel, National Aviation Facilities Experimental Center, Atlantic City, N. J.

Airborne Flame Generator. In the Great Lakes Winter Storms Project (Weickmann, 1973), Patten-Mark series airborne flame generators (Patten et al., 1971) were used to deliver the AgI aerosol. The aircraft, a DC-6 and a Queen Air, flew at approximately 200 mph (88.8 m sec^{-1}); therefore we conducted this experiment at a similar flow rate in the wind tunnel.

Pyrotechnic Generator. NOAA/ERL Experimental Meteorology Laboratory (EML) has used the airborne pyrotechnic cloud seeding system since 1968 (Simpson and Woodley, 1970). However, little investigation of the particles' chemical and physical properties has been done. The terminal velocity of the pyrotechnic flares at the inflaming point is approximately 150 mph (66.6 m sec^{-1}). Thus, our investigation of these seeding particles was done at a similar airflow.

Flame Generator-Modified Tests. The arrangement for these tests was the same as for the airborne flame generator, except instead of an AgI-acetone solution we used either solid AgI or two solid AgI-NaI mixtures. Gasoline or acetone was used as the fuel.

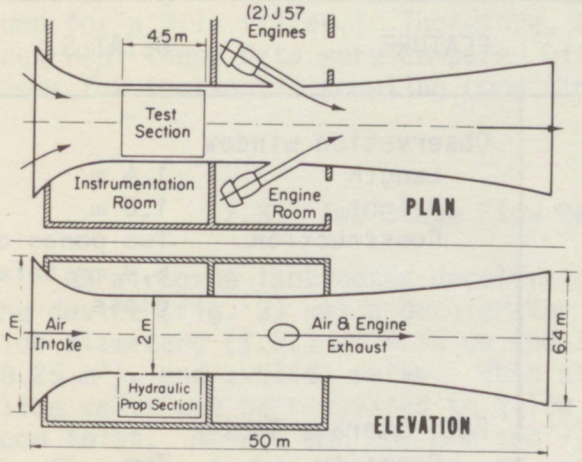

Figure 2. The diagram of the wind tunnel.

2. AEROSOL SAMPLING

Sampling an aerosol in a rapid airstream having anisokinetic flow conditions at the sampling orifice can cause a serious error in the particle size distribution (Watson, 1953). Isokinetic conditions occur only when the flow carrying the aerosol enters the sampling orifice without accelerating or decelerating, converging or diverging, thus, the air flows uniformly without turbulence. However, it is difficult to achieve an absolutely isokinetic condition when the wind speed is 200 mph (88.8 m sec^{-1}) and sampling flow capacity is limited to 10 to 20 ℓ min^{-1}. To obtain sufficient data for evaluation and comparison of sampling results, we used four different sampling techniques.

2.1. One-Stage Decelerating Sampler

From theoretical calculations, we designed a cone having an orifice diameter of 1.75 mm and a 7° angle for mounting on the 47 mm Millipore filter holder; the cone decelerated the flow rate to 12 ℓ min^{-1}, which means we could get approximately isokinetic conditions by using the same sampling flow rate. The filter holder was 1.75 m from the AgI generator. Both Millipore filters and Nuclepore filters (0.1 μ pore) were used to collect aerosol samples.

Table 1. FAA Wind Tunnel Specifications

FEATURE	DETAILS	FEATURE	DETAILS
Location	Atlantic City, N.J.	Observation window	
Wind Tunnel		Length	1.4 m
Length	50 m	Height	1.0 m
Test Section		Construction	Two panes of 6.4 mm safety glass
Length	4.5 m		
Diameter	2 m		
Access Door		Fuel Storage Tanks	
Height	4.5 m	Quantity	Two
Width	1.4 m	Total Capacity	20,000 gallons
Maximum air speed	650 mph (289 m/sec)	Air Receiver Tank	
Maximum simulated		Capacity	12.7 m^3
Altitude	400 m	Normal pressure	827,280 Pa (120 psi)
Turboject Engines		Power Available	
Ouantity	Two		115 V, single phase, 60 cycle
Type	J-57-F19W		115 V, single phase, 400 cycle
Manufacturer	Pratt and Whitney		115 V, 3 phase, 60 cycle
Maximum thrust per engine	4761 g		220 V, 3 phase, 60 cycle
Maximum rate of fuel consumption per engine	3571 g/hour		26 V, single phase, 400 cycle
			28 V dc

2.2. Anisokinetic Sampler

To collect the aerosol directly, we placed an open filter holder with a 47 mm filter (0.1μ) at the same distance as the previous sample. The sampling flow rate was 16 ℓ min^{-1}. (The maximum capacity of the pump for a 0.1μ filter.) Therefore, a strong anisokinetic condition occurred; these data were compared with the particles' size distributions for isokinetic sampling conditions.

2.3. Two-Stage Flow Decelerating System

An airborne isokinetic decelerator was developed by Eyre (1974). The device (fig. 3) has a decelerator boom (a cone 6.6 m long with inside diameters (I.D.) of 6.55 cm and 19.0 cm at each end), sampling tank (0.25 m^3), and a slide valve. When sampling at certain wind speeds, the slide valve can be regulated to allow an isokinetic flow through the boom inlet. At 200 mph (88.8 m sec^{-1}) flow, the system can decelerate the flow rate isokinetically to 25 mph (11.1 m sec^{-1}). Inside the sampling tank, a filter sampler with another decelerator cone collects the aerosol. The sampler cone (7°, I.D. = 2.75 mm and 47 mm) further reduces the flow from 25 mph (11.1 m sec^{-1}) to a sampling rate of 8 ℓ min^{-1}. Thus an isokinetic condition was achieved by using 8 ℓ min^{-1} sampling rate.

2.4 Thermal Precipitator

A thermal precipitator was placed in the tank of the Eyre isokinetic decelerator. Electron microscope sampling screens with Formvar film collected the aerosols. The sampling rate was set for 3 mℓ min^{-1}

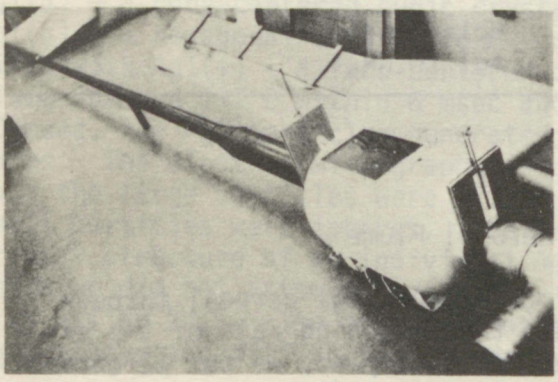

Figure 3. The airborne isokinetic decelerator developed by Eyre.

and sampling time was 4 min; thus, the sampling condition was not isokinetic even when the sampler was set inside the tank where the air flow was decelerated to 25 mph (11 m sec^{-1}). Nevertheless, the thermal precipitator had its merits. The collecting efficiency was 99 percent and the sampling screen could be examined directly by transmission electron microscope (TEM). These results were compared with the samples collected on filters, which need to be transferred to the screen for SEM examination. There is always the danger of loss or of changing the aerosol's character during a transfer process.

3. AEROSOLS PRODUCED BY AIRBORNE FLAME GENERATOR

ERL's Research Flight Facility (NOAA) developed an airborne steady-state silver iodide flame generator for mounting on the wingtip of an aircraft (Patten et al., 1971). Acetone is the fuel as well as the solvent for the AgI. Sodium iodide (NaI) or ammonium iodide (NH_4I) is added to form a homogeneous solution. The compositions of the solutions are shown in table 2.

Table 2. Composition of AgI Solutions

AgI-NaI System		AgI-NH_4I System	
AgI	299.46 g	AgI	308.72 g
NaI	100 g	NH_4I	98.70 g
Acetone	19 ℓ	Acetone	19 ℓ
AgI concentration by weight	2 %	AgI concentration by weight	2 %
Weight ratio AgI to NaI	3 to 1	Weight ratio AgI to NH_4I	3 to 1
Molar ratio AgI to NaI	2 to 1	Molar ratio AgI to NH_4I	2 to 1

3.1 Quenching of the Aerosol Plume

The flame generator was designed to produce AgI aerosol through the vapor-solid transition. To measure the quenching rate of the exhaust AgI vapor at 200 mph (88.8 m sec^{-1}) wind speed, we put 12 chromel-alumel thermocouples in a row from 0 to 34 inches (86 cm) away from the generator's exhaust cone (fig. 4). When the AgI-acetone solution was

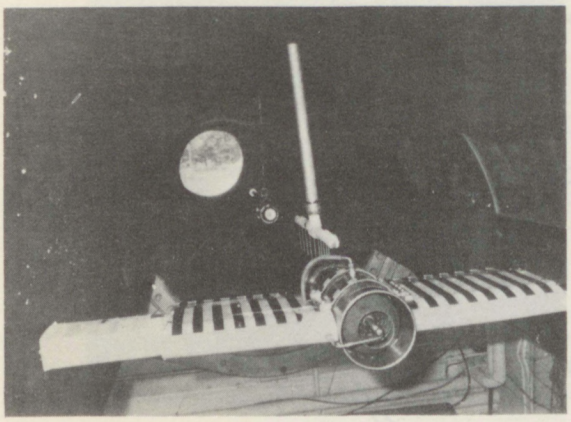

Figure 4. The flame generator mounted in the wind tunnel.

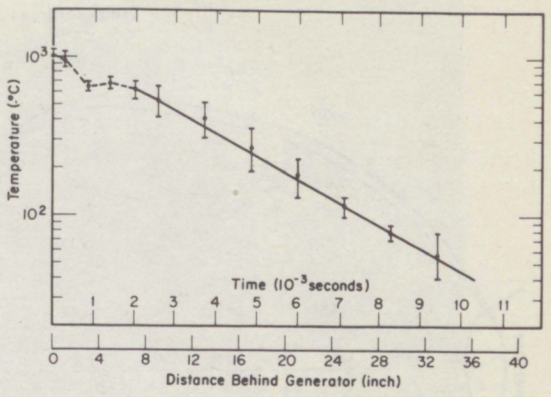

Figure 5. Temperature profile of the generated aerosol.

injected at 0.6 ℓ min^{-1} into the generator and combusted, the flame temperature was approximately 1000°C. There was practically no temperature difference between the AgI-NaI and the AgI-NH_4I solution. Figure 5 shows the temperature profile of the flame and the cooling rate of the generated plume. The thermocouple series was then turned 90° to measure the temperatures in the flame's cross section. The flame was symmetric; figure 6 shows its three-dimensional temperature diagram. Both figure 5 and figure 6 indicate the quenching rate of the plume was so rapid that the AgI vapor reached supersaturation within milliseconds.

3.2 Crystal Forms of AgI Particles

According to Burley (1963), AgI vapor condensing above 147°C forms AgI(α) — a body-centered cubic crystal form. Between 135 to 147°C, pure AgI(β) — a hexagonal crystal form — is stable. Below 135°C, AgI(β) is mixed with AgI(γ) — a face-centered cubic crystal. Because the exhaust plume reached 147°C within 6 msec and cooled to ambient temperatures in 10 msec, the AgI particles generated should have been in the β and γ forms. The electron micrographs (figs. 7 and 8) of the aerosol show that the large particles were either hexagons or triangles, and the small particles were spheres. The method of segregating the internal crystal structure of an individual AgI particle is X-ray defraction, which we did not attempt because the generated AgI aerosol was mixed with NaI or NH_4I. The structure of the resulting particle would be very complicated and difficult to study.

In classical theory of ice nucleation, epitaxy was considered as the most important mechanism. Thus, AgI(β), whose hexagonal space lattice

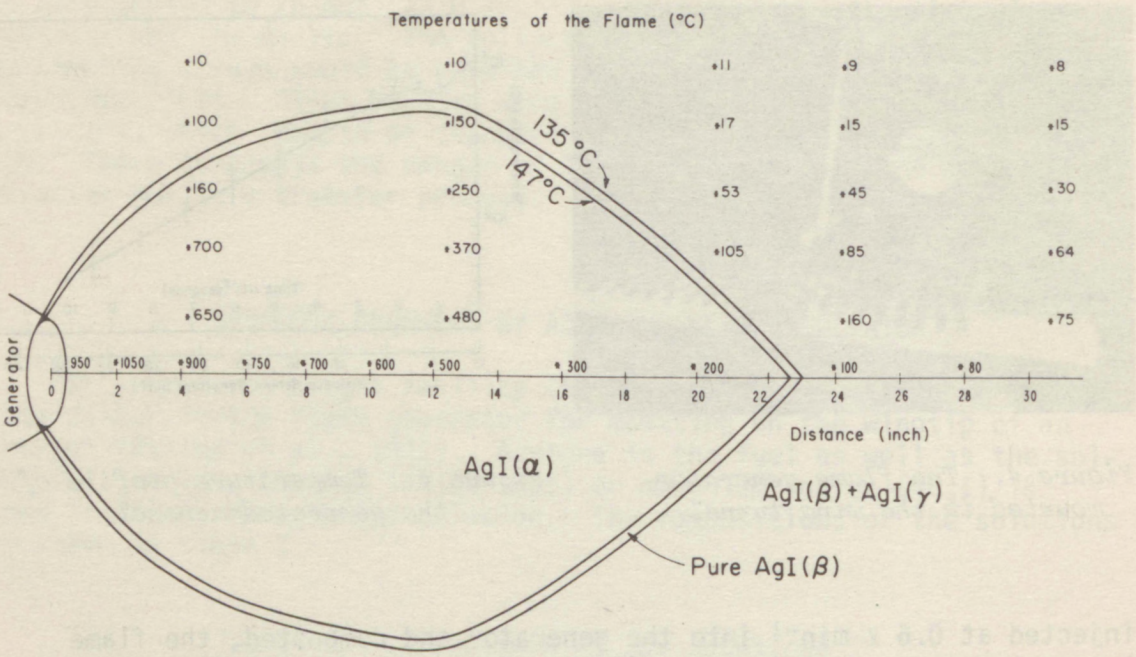

Figure 6. Temperature diagram of the flame.

closely resembles ice, was hypothesized to be the most active ice nucleus among all three forms. Consequently, generating methods that could produce more β-forms were considered desirable. We now realize that ice nucleation includes three mechanisms: deposition, condensation freezing, and contact nucleation. Epitaxial growth is only important in deposition nucleation. Furthermore, Isono and Schizaka (1968) found that AgI(α) and AgI(γ) were more efficient deposition nuclei than AgI(β). Fletcher (1959) claimed that on a single AgI(β) crystal, the prism face was more active than the basal face. Therefore, for sublimation nuleation by the epitaxial processes, it is more important to match the two-dimensional crystal lattice on the faces than the three-dimensional general resemblence of the space lattice.

Since AgI(β) is not a superior ice nucleus over its allotropic forms and all three polymorphs of AgI are active ice nuclei (Isono and Shizaka, 1968), we do not discriminate between the individual forms in the investigation in this report. We place instead more emphasis on the size and chemistry of the particles.

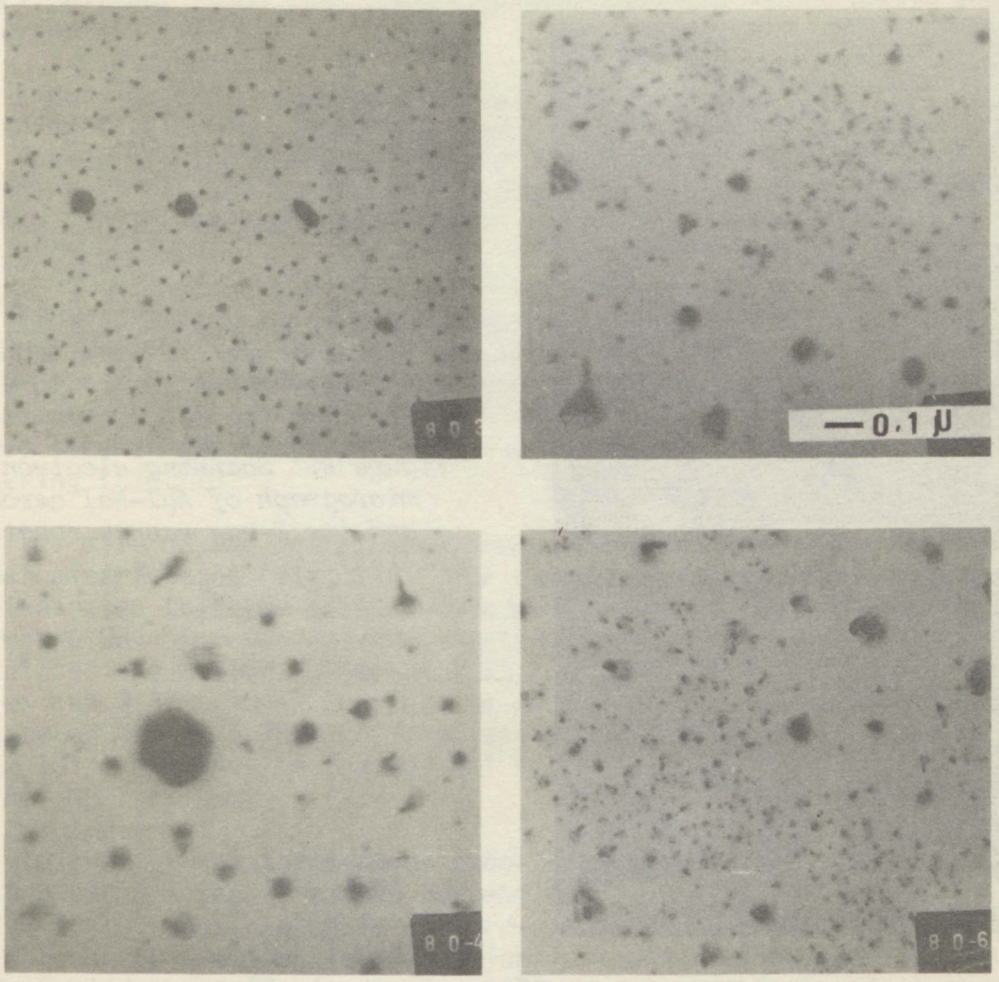

Figure 7. Electron micrographs of the generated AgI-NaI aerosol.

3.3 Aerosol Size Distribution

To investigate whether we had properly collected suitable amounts of the aerosol in the sample, we used the electron microscopes at the nearby Army Electronic Command Laboratories in Fort Monmouth, N.J. All the usable samples were then brought to Boulder, Colorado, for a thorough study at the Atmospheric Physics and Chemistry Laboratory (APCL). APCL has a Coates and Welter Scanning Electron Microscope (SEM) with a resolution of 250 Å; we also used the National Center for Atmospheric Research's Zeiss and RCA transmission electron microscopes (TEM), which have a resolution of 20 Å. Samples on the screens and filters can be directly inserted in the SEM for observation; we used it for a quick, preliminary investigation. However, we had to use the RCA or Zeiss TEM to include all the fine particles for analyzing their size distribution.

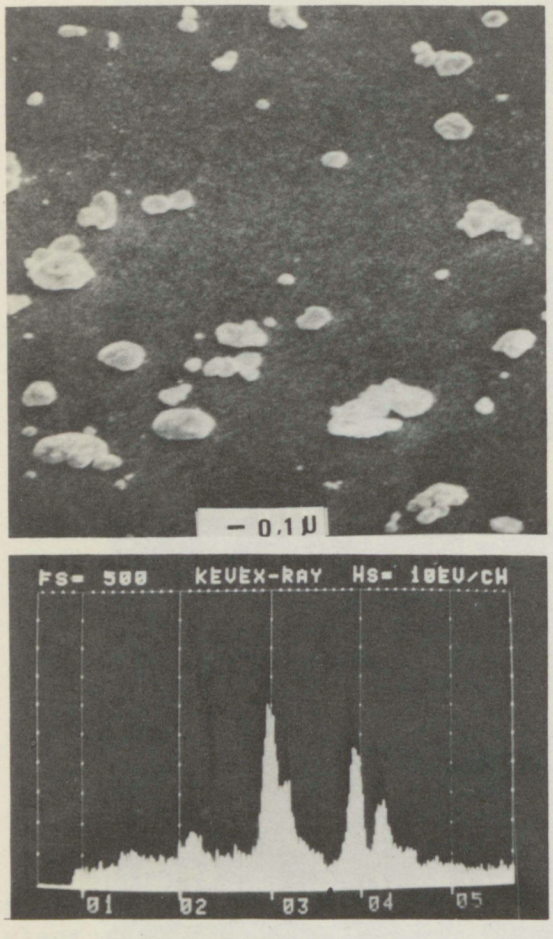

Figure 8. Scanning electron micrograph of AgI-NaI aerosol and its X-ray energy spectrum (XES).

For study with the TEM, specimens must be on transparent film, mounted on the electron-microscope screen. Aerosol samples collected on the screens with the thermoprecipitator can be directly observed and photographed by the TEM. The samples on Nuclepore or Millipore filters must be replicated with a layer of silicon monoxide (SiO) coating and transferred to the TEM screen by dissolving the filter with a solvent (Frank et al., 1970). The transparent SiO film with these aerosol replicas mounted on the screen then can be examined with the TEM.

The particle size distribution shows no statistical difference between one-stage and two-stage methods of isokinetic sampling; samples collected by the thermal precipitator also yielded a similar distribution. However, the open filters that collected the aerosols anisokinetically showed the distribution shifted to larger sizes than for the other three methods. These results agree with a tentative semi-empirical

theory (Watson, 1953) that covers errors caused by anisokinetic sampling of aerosols.

Figure 9 shows the size distribution of the AgI-NaI particles. The mean diameters of the isokinetic and the anisokinetic particles differ by a factor of almost eight. Figure 10 shows the size distribution of the AgI-NH_4I particles; their mean diameter is 0.004μ for the isokinetic samples, while for the anisokinetic samples, it is 0.014μ, or a factor of 3.5 larger.

Figures 11 and 12 show the electron micrographs of the AgI-NaI and AgI-NH_4I aerosols collected by the thermal precipitator. Note that these particles are present individually without aggregation. However, the samples collected on an open filter (without the isokinetic cone) showed some of the large particles were the product of aggregation and sintering (fig. 13).

The size of the AgI aerosol produced by the generator showed a log-normal distribution (fig. 14). The cumulative size distribution (fig. 15) indicates that the median diameter was 0.008μ for the AgI-NaI system and was 0.004μ for the AgI-NH_4I system. Using the median radius, we calculated the median volume as 2.73×10^{-19} cm^3 for the AgI-NaI particles and 3.37×10^{-20} cm^3 for the AgI-MH_4I particles. Since the density of AgI is 5.76 g cm^{-3}, we estimate that 1 g of AgI can produce 6.4×10^{17} particles in the AgI-NaI system and 5.1×10^{18} particles in the AgI-NH_4I system.

In conclusion, the aerosol produced by the airborne generator at 200 mph (88.8 m sec^{-1}) has 90 percent of its population in the 3×10^{-3}μ to 3×10^{-2}μ range, which is one order of magnitude smaller than the radii found in previous investigations using a similar generator but at a lower wind speed (Davis et al., 1973; Mossop and Tuck-Lee, 1968).

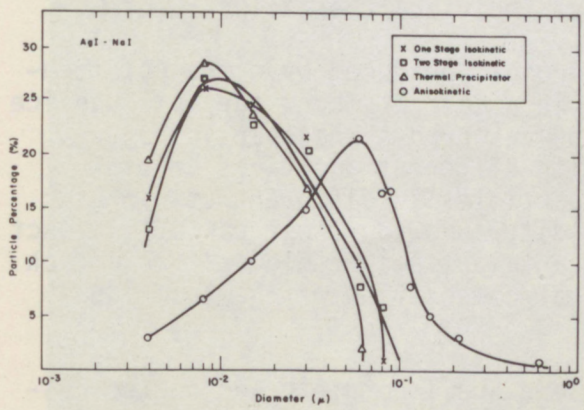

Figure 9. Size distribution of AgI-NaI aerosols which were collected by different methods.

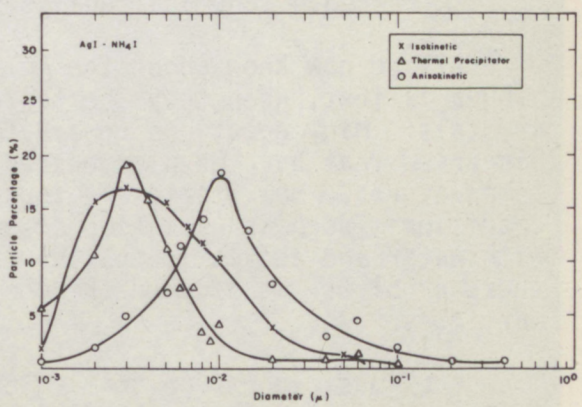

Figure 10. Size distribution of AgI-NH_4I aerosols which were collected by different methods.

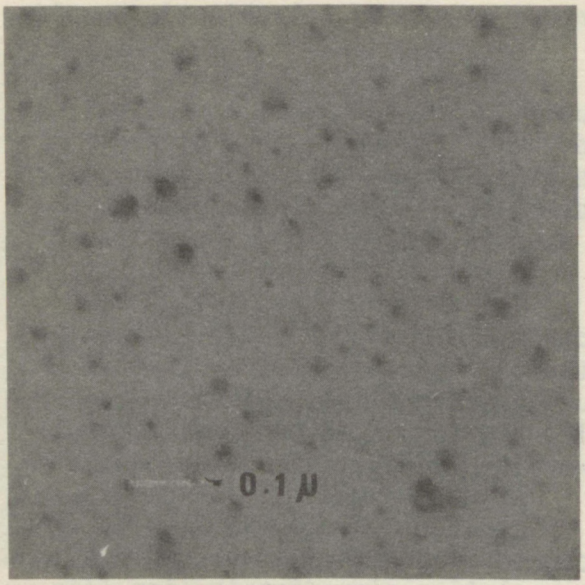

Figure 11. Electron micrograph of AgI-NaI aerosol sampled with a thermal precipitator.

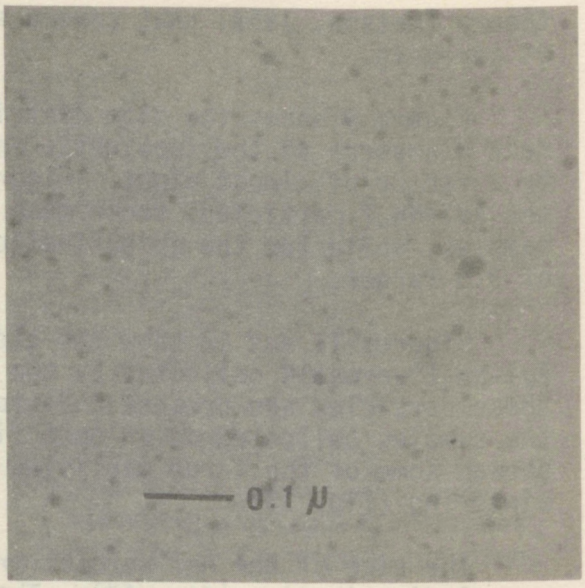

Figure 12. Electron micrograph of $AgI-NH_4I$ aerosol sampled with a thermal precipitator.

This smaller particle may be caused by the fast airflow dispersing the exhaust vapor thinner; the quick quenching rate solidifying the particles quicker; and the immediate sampling preventing the particles coagulating. Of course, the isokinetic sampling, as we have found, can lead to a more accurate measurement.

3.4 Chemical Analysis of Individual Particles

All we now know about the AgI aerosols produced by different techniques is that, when they are tested in a cold chamber, they produce ice crystals. Many questions remain to be answered. What particles are dispersed that have been combusted with different additives at high temperatures? How stable are these particles in different atmospheric conditions, such as radiation or humidity? How do these particles react with water and act as ice nuclei in certain types of clouds? To attack these problems, we studied the chemical composition of the individual particles.

Previous reports on these questions are incomplete and controversial. Mason and Hallett (1956) investigated electron defraction patterns of AgI aerosols that were vaporized from an AgI-NaI dry mixture; they could not find hexagonal AgI(β), so they deduced that the particles were either cubic AgI(γ) or NaI. Pena and Caimi (1967) analyzed the aerosol

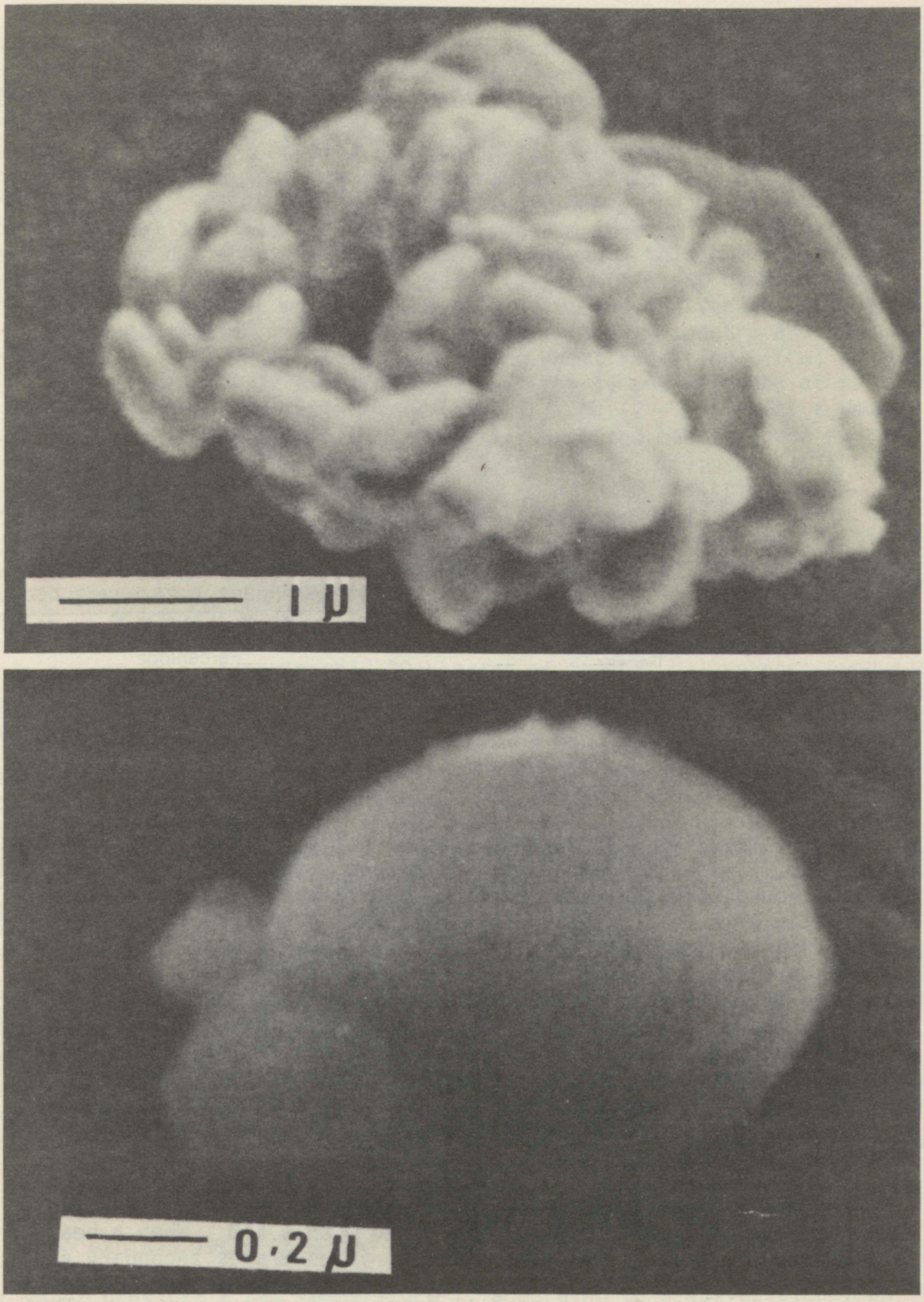

Figure 13. Scanning electron micrograph of (a) AgI-NaI aerosol and (b) AgI-NH_4I aerosol, sampled anisokinetically.

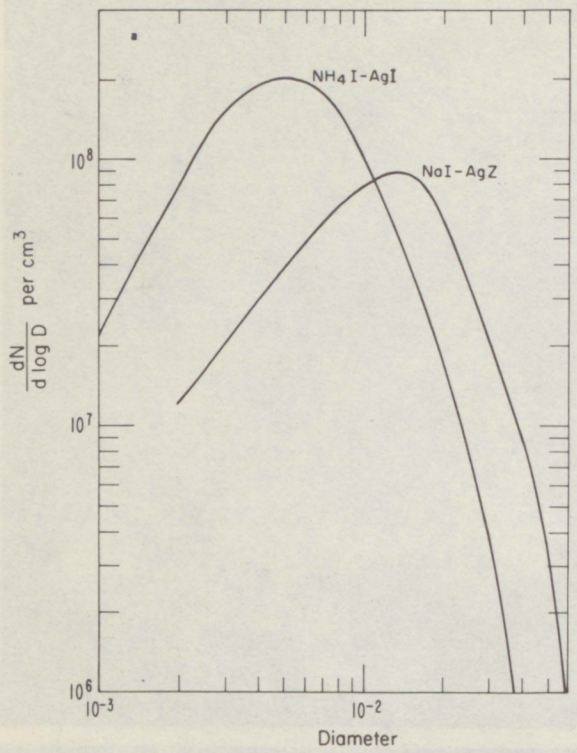

Figure 14. Size distributions of the aerosols: AgI-NaI and NH_4I.

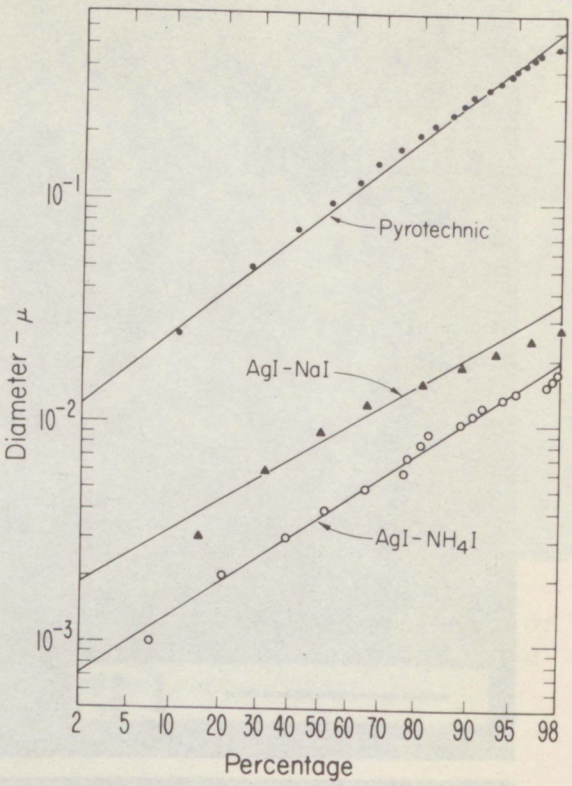

Figure 15. Cumulative size distributions of the aerosols.

produced by spraying a 35 percent acetone solution of AgI and KI (molar ratio 2 to 1) without heating it. To no one's surprise, their chemical analysis found that the total aerosols consisted of AgI and KI in a molar ratio of 2 to 1. Their X-ray diffraction pattern of the particles matched neither AgI's nor KI's. Therefore, they deduced that a double salt was present. Mossop and Tuck-Lee (1968) found that the particles generated by burning an acetone solution of AgI-NaI consisted of a mixture of AgI and NaI either separate or combined. Nevertheless, these results cannot be compared with one another because the aerosols were produced by different methods. Therefore, to know the composition and properties of the aerosols produced by our seeding technique, we must analyze the aerosol collected at a realistically simulated seeding condition.

For the elemental analysis of the generated particles, we used an X-ray Energy Spectrometer (XES) interfaced with a SEM. When a beam of high-energy electrons scans the specimen, it generates secondary electrons and backscattered electrons; a detector receives the information

and produces an image of the specimen's surface. Meanwhile, the impinging electrons can also collide with a bound electron around the specimen atom and free it from its normal orbit to create a "hole." An electron from a higher energy orbit fills in this "hole" and emits well-defined quantum energy. As a result, from the X-ray radiation we can identify the elements in the specimen and from radiation intensity we can measure their quantity. By using the combination of SEM and XES, we can observe the individual particle — its size, shape, and surface structure; at the same time, we can identify its elements. However, this precise instrument has three limitations at present: (1) a particle's diameter must >250 Å: (2) its atomic number, Z, must be >10; and (3) the analysis is only semiquantitative. Examples of the X-ray energy spectra are shown in figure 16: (a) NH_4I, where only iodine emits radiation, I(Lα) at 3.94 keV, I(Lβ) at 4.22 keV; the hydrogen (Z = 1) and nitrogen atoms (Z = 7) do not yield detectable X-rays; (b) NaI, Na (Z = 11) emits a weak X-ray at 1.07 (Kαβ); (c) AgI, it is easily detected because both Ag and I have intense radiation (Ag Lα at 2.98, Ag Lβ at 3.15); (d) KI, K can also be identified by its Kα at 3.31 and Kβ at 3.59 radiation lines. For the AgI aerosol flame generator, NH_4I, NaI, or KI is added into AgI acetone solution to form a homogeneous phase. If only for identifying the aerosols by XES, KI is a better choice as an additive because it can serve as a secondary tracer.

Since the SEM-XES limits the particle's diameter to >0.02μ, it is unfortunate that approximately 90 percent of the AgI-NaI aerosol produced by the flame generator was smaller than this size and cannot be studied by this method. We therefore could obtain the X-ray spectra (fig. 17) for only the larger particles (d > 0.02μ). When the AgI-NaI solution was used, the generated aerosols shows no Na in the particles d > 0.5μ. However, when d < 0.5μ, a low intensity X-ray at 1.07 keV, which is Na's Kαβ radiation was detected. Furthermore, as the particles got smaller, the iodine peaks got stronger, indicating more NaI was present; however, no pure NaI particles were detected. Figure 18 shows the relationship between X-ray intensity of AgI-NaI particles and their size. The X-ray intensity depends not only on the specimen's quantity, but also on its topography and matrix, which are unknown factors here. In addition, the conditions influential to the analysis (such as the accelerating voltage, current of the electron beam, magnification, and X-ray detector's distance) may not always be absolutely constant for every measurement. Therefore, the analysis was semi-quantitative. The data points on the graph are the 10 percent trimmed mean and the line is the 10 percent trimmed range. However, from these experimental data, we can draw a general conclusion: the detectable surface of large particles (d > 0.5μ) was covered with only AgI, while smaller particles (d < 0.5μ) consisted of both AgI and NaI.

To explain these results, we must examine the thermodynamic properties of all the compounds involved. Figure 19 shows the relationship of vapor pressure P and temperature T, according to Clausius-Clapeyron

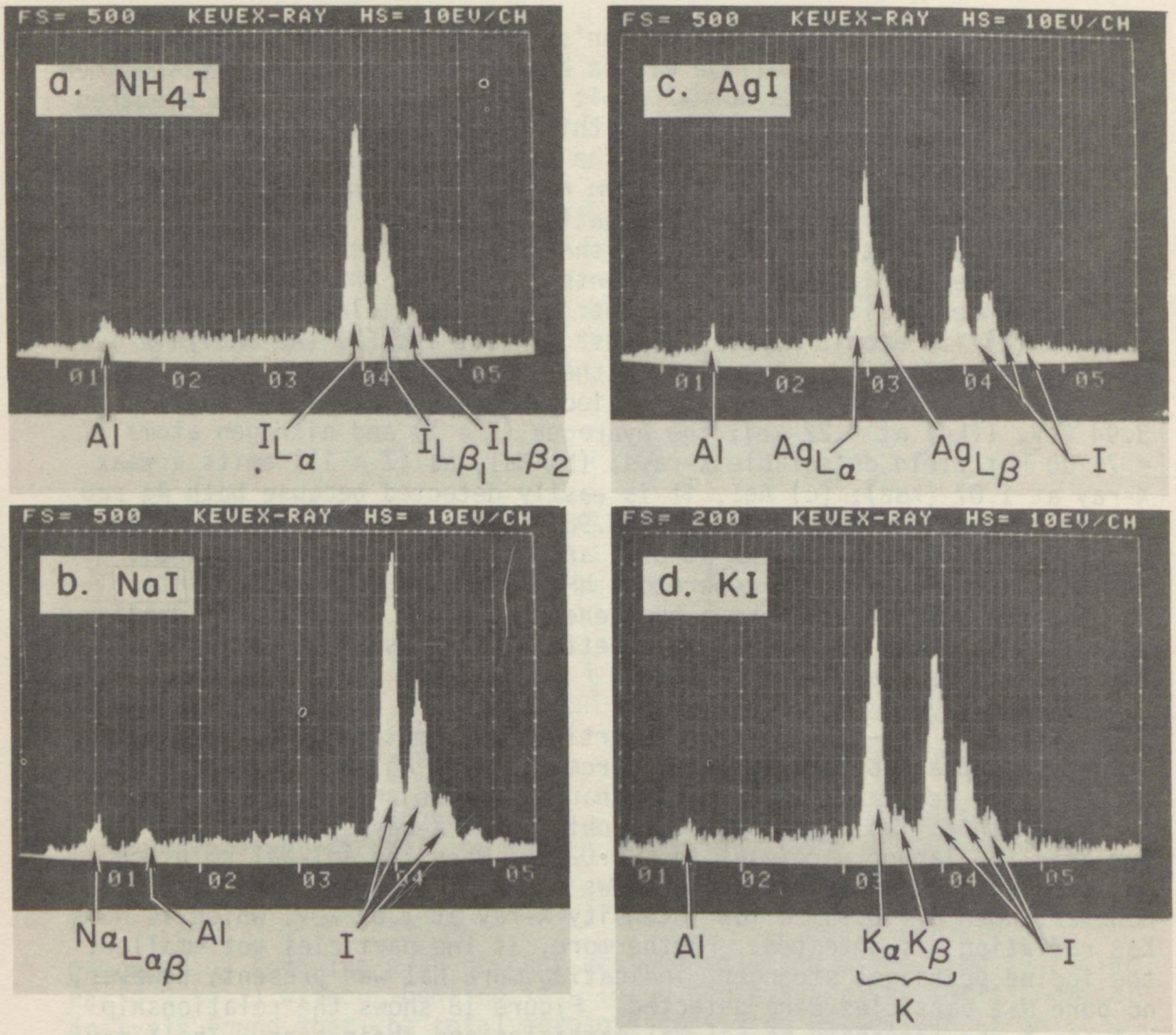

Figure 16. XES of (a) NH_4I, (b) NaI, (c) AgI, and (d) KI.

equation, $\Delta \log P = \Delta H/R\Delta T$, where ΔH is either the heat of evaporation or the heat of formation. The saturation vapor pressure of NaI is slightly higher than that for AgI at a given temperature. Thus, the NaI and AgI solidify together simultaneously to form a solid solution. In addition, AgI partially decomposes above its melting point (550°C); free Ag and I_2 vapor are products of the exhaust plume and will recombine to form AgI vapor when they cool. However, the vapor pressure required to form AgI by reaction of Ag and I is so much higher than that required to form either AgI particles or NaI particles from its vapor that Ag and I_2 only recombine later at a lower temperature. The freshly

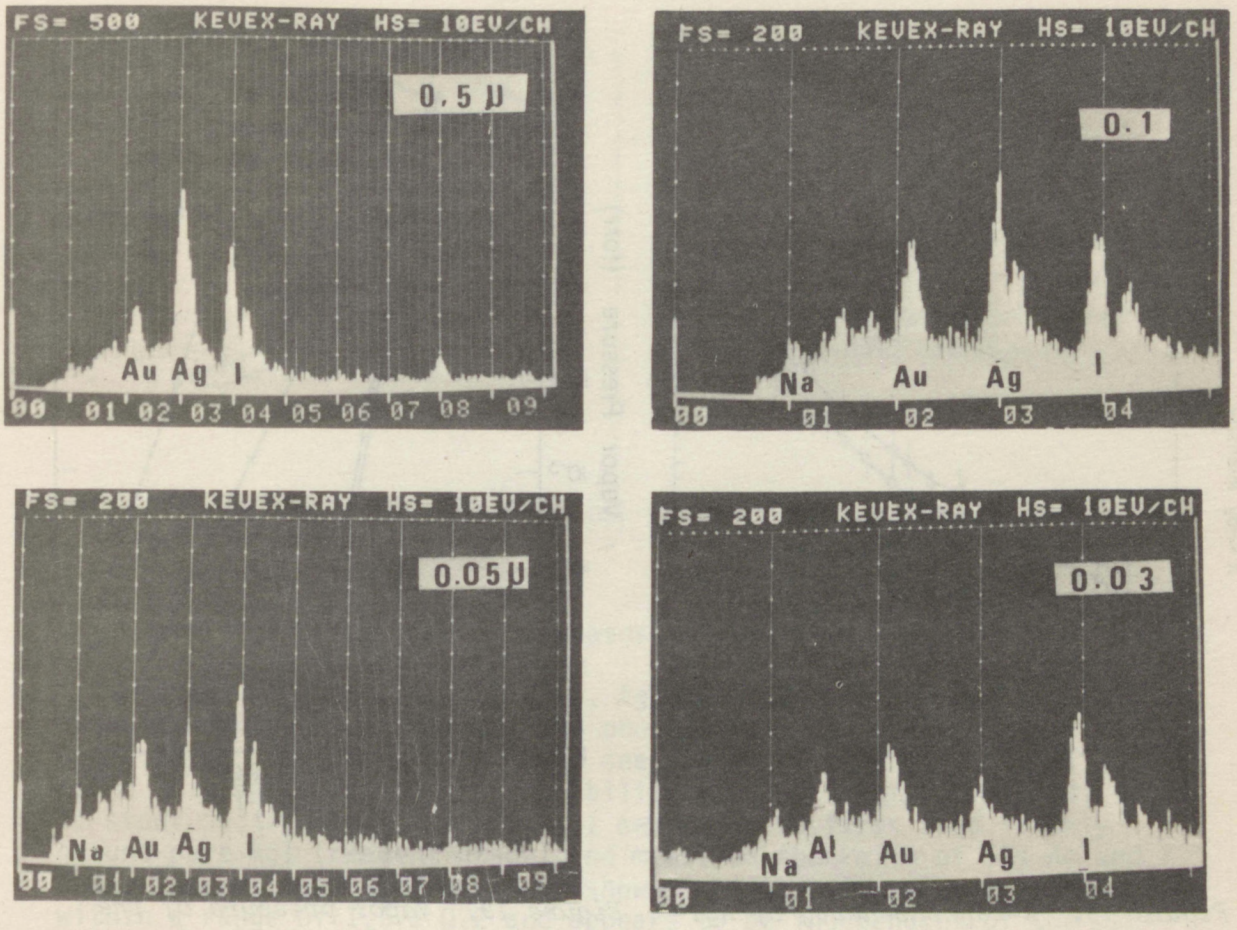

Figure 17. XES of AgI-NaI aerosol with different sizes.

formed AgI vapor then deposits on the already existing AgI-NaI particles by heterogeneous nucleation and envelopes them. Thus the large particles, whose pure AgI coating is thick enough to prevent electron beams from penetrating it, fail to emit X-ray radiation of the enclosed NaI; however, the small particles with a thinner coating show X-ray radiation of both AgI and NaI.

When we used the AgI-NH_4I solution in the flame generator, the particles were uniformly smaller than those of the AgI-NaI systems. Again, 95 percent of the particles were too small to be detected by XES. To understand the formation of these fine particles, we need to study the thermodynamics of the vapor-solid transition as shown in figure 19. The NH_4I vapor reaches saturation at a lower temperature than AgI. When

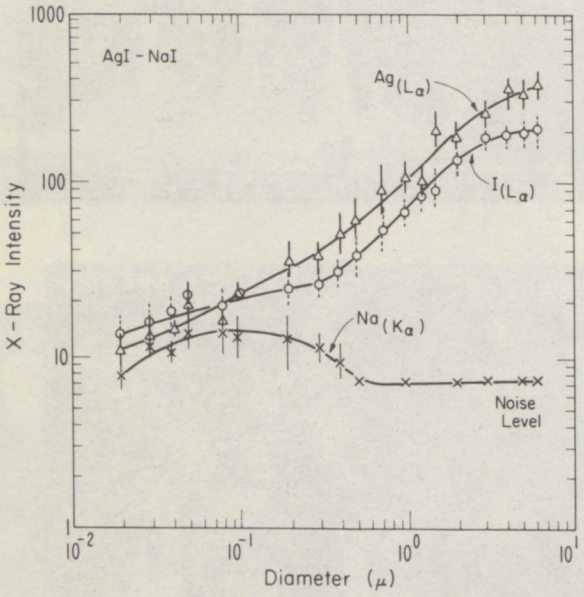

Figure 18. X-ray intensity of AgI-NaI particles.

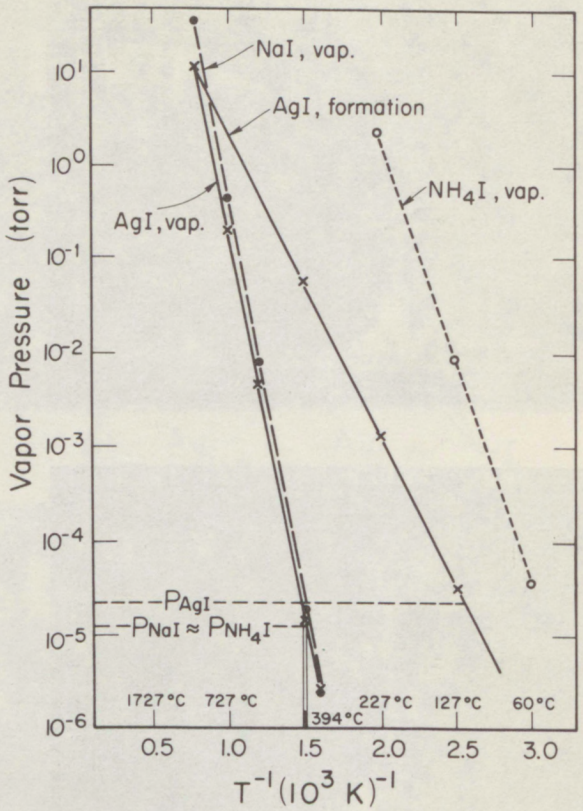

Figure 19. Vapor pressure of the iodides at various temperatures.

the exhaust plume cools down, AgI solidifies by homogeneous nucleation to form fine particles and then the NH_4I vapor deposits on the AgI surface. Since we used less NH_4I than AgI (mole ratio 1 to 2), and since NH_4I is a thermally unstable compound that decomposes into NH_3 and HI and loses portions in the flow, we can expect that there was not enough to give as thick a surface coating on the AgI particles.

Figure 20 shows the experimental results of the relationship between the particle size ($d > 0.02\mu$) and X-ray intensity. Unfortunately, N and H are not detectable by XES; thus, the ammonium contribution to the particles cannot be measured. However, we can observe there was no sudden change in the ratio between the X-ray intensity of Ag and I. We can reasonably deduce that large and small particles have similar surface composition, and that the aerosols produced by the AgI-NH_4I systems were AgI particles that were covered with either a thin layer or spots of NH_4I.

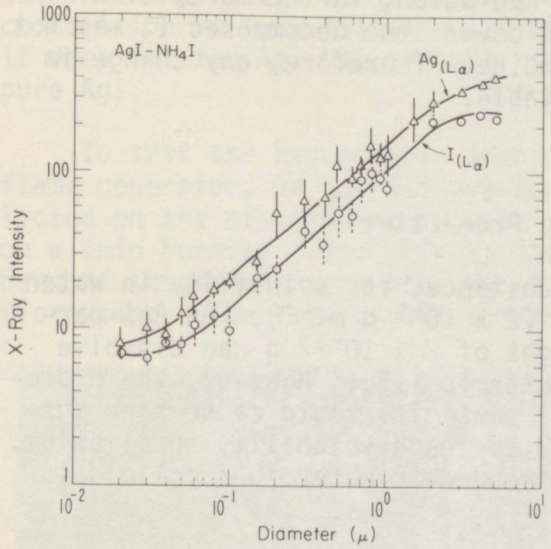

Figure 20. X-ray intensities of AgI-NH_4I particles.

3.5 Photostability

In the photographic industry, AgI has been used as a photodetector because of its sensitivity to the photons that decompose it into silver and iodine. When used as a cloud seeding agent, Reynolds et al. (1951) found that AgI's ice nucleation ability was deactivated by irradiation. To study photodecomposition of AgI aerosols, we first used freshly ground pure AgI (reagent grade) and measured the ratio of its Ag and I X-ray intensities; the result is shown in figure 21. The ratio (top) is within a range of 1.5 ± 0.2 and appears to be independent of the particle's size. If AgI is decomposed by radiation, the iodine produced would evaporate and Ag would remain; as a result, the ratio of X-ray intensity between Ag and I should increase. This is indeed what we found when we irradiated AgI particles with sunlight or ultraviolet (UV) light (2573 Å) for 2 hours. The average increase in the ratio was approximately 15 percent.

Next we used the same method to study the aerosols that were produced by the AgI-NaI mixture (fig. 21, middle). As we have mentioned previously, the ratio of the X-ray intensity of Ag to I decreased as the particles' size decreased, because the small particles had a thin AgI coating and the larger ones had a thick AgI coastng. As these particles were irradiated with sunlight or UV light, the Ag to I ratio increased for all sizes; however, the degree seems more intense for the fine particles than for the coarse ones.

When the AgI-NH_4I aerosols were investigated for their photostability (fig. 21, bottom), we observed no significant increase in the ratio of Ag to I. If we apply our findings that the AgI-NH_4I aerosols are partially or completely covered with NH_4I, it is easy to understand

that the AgI may be shielded from the radiation; furthermore, even if the photons penetrate through the NH_4I cover, the decomposed I_2 may not escape easily and Ag and I could recombine. Therefore, any change in the ratio of Ag to I would be undetectable.

3.6 Hygroscopic Properties

Silver iodide is a hydrophobic substance; its solubility in water is approximately 2 parts per trillion (2×10^{-9} g $m\ell^{-1}$). An AgI particle with a diameter of 0.1μ and weight of 2×10^{-18} g can dissolve completely in a water drop whose diameter is >15μ. However, the hydrophobic character of the surface of AgI particles could cause high surface tension, and they would need time to reach solubility equilibrium. Thus, fine AgI particles are often suspended in water in a colloidal state for an indefinite time.

When AgI is mixed with NaI or NH_4I to produce aerosols, the hygroscopic property of the particles depends on the construction of their components. If the combination of AgI and NaI (or NH_4I) is a homogeneous solid solution, this will reduce the hydrophobic character of the AgI and the new compound will be more soluble than AgI alone. If the AgI is coated with a hydrophilic component, such as found in the AgI-NH_4I aerosol, the surface of the particles would be hygroscopic, but

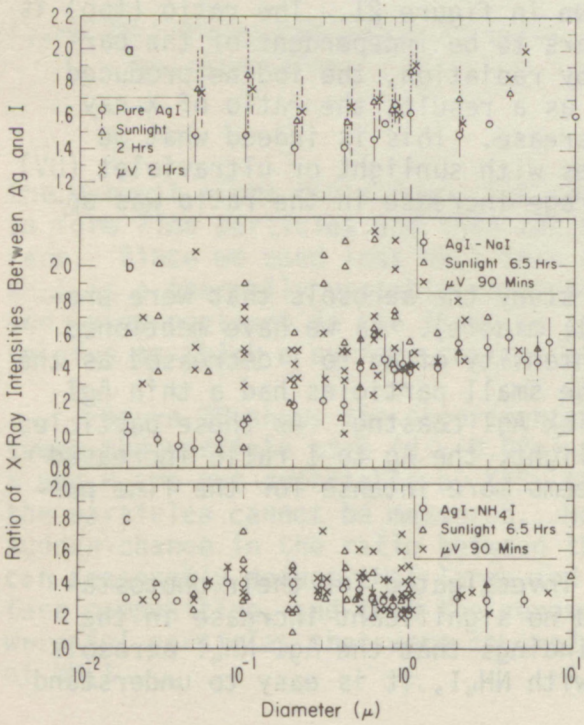

Figure 21. Ratio of X-ray intensities between Ag and I, effected by radiation: (a) AgI; (b) AgI-NaI; (c) AgI-NH_4I.

the inner AgI would remain hydrophobic. Furthermore, if the particle's composition is such that the AgI envelopes the hydrophilic portion as it does for the AgI-NaI aerosol, then it would be as hydrophobic as pure AgI.

To test the hygroscopic properties of the aerosols produced by the flame generator, we carried out three experiments using the samples collected on the electron-microscope screen, where the particles were set on a thin Formvar film. First, the screens were placed in a small chamber and suspended over water for 1 hour and then examined by an electron microscope. The results are shown in figure 22: (a) AgI-NaI particles

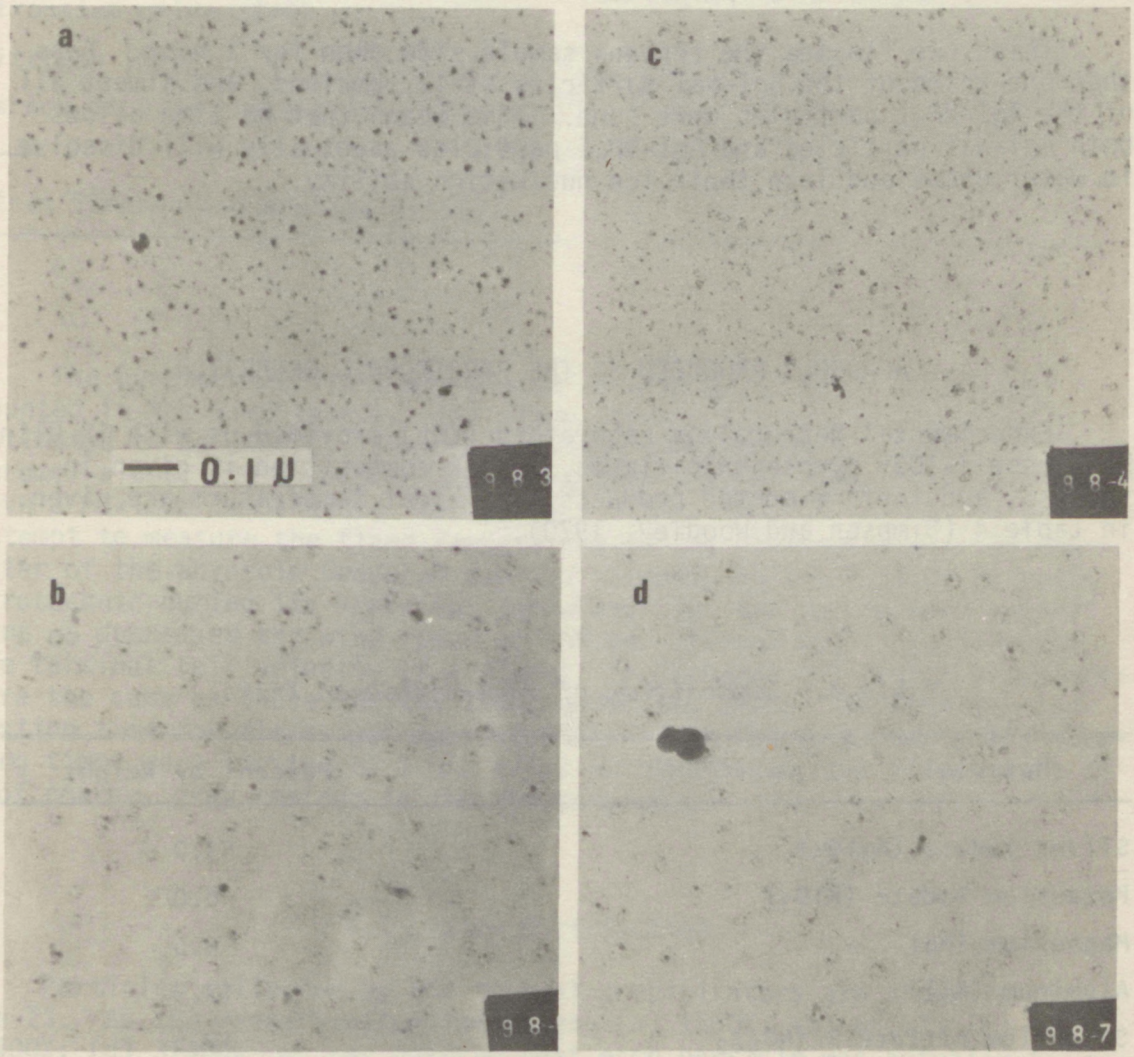

Figure 22. Electron micrographs of particles treated with water: (a) AgI-NaI exposed to water vapor; (b) AgI-NH_4I exposed to water vapor; (c) AgI-NaI contacted with water; (d) AgI-NH_4I contacted with water.

showed little effect from the water vapor; (b) AgI-NH_4I absorbed moisture and formed a drop, which after it dried left a ring of dissolved residue around the insoluable particles. The experiment indicates that the AgI-NH_4I aerosol is more hygroscopic and thus more effective as condensation-freezing nuclei than the AgI-NaI aerosol.

Second, the same screens were floated on water with the sample side up for 1 hour. Water could filter through the Formvar film and contact the particles. The AgI-NaI particles (fig. 22 c) were partially dissolved, and the AgI-NH_4I (fig. 22 d) particles were mostly dissolved and washed away. This indicates that in water AgI-NaI particles survive better than the AgI-NH_4I particles.

Third, we floated the screens sample side down for 1 hour. Less than one-third of the AgI-NaI particles still remained, and almost all of the AgI-NH_4I particles were gone. This means that as time allows both AgI-NaI particles and AgI-NH_4I particles eventually will dissolve in water drops and lose their ice nucleation ability.

4. AEROSOLS PRODUCED BY THE PYROTECHNIC GENERATOR

Experimental Meteorology Laboratory (EML) provided us with 12 Olin-Mathieson X-1055 pyrotechnic flares. Their composition is given in table 3, and their expected products at ambient temperature are given in table 4 (Simpson and Woodley, 1970).

Table 3. Composition of Olin-Mathieson X-1055

Material	Percent by Weight
Silver iodate ($AgIO_3$)	53.0
Potassium iodate (KIO_3)	8.0
Magnesium (Mg)	5.6
Aluminum (Al)	12.9
Strontium nitrate $Sr(NO_3)_2$	10.5
Polyester binder	10.0

Table 4. Expected Exhaust Products of the Olin-Mathieson X-1055[1]

Compound	Amount per 100 gm mixture
Silver iodide (AgI)	44.0
Potassium iodide (KI)	6.1
Magneisum oxide (MgO)	9.5
Aluminum oxide (Al_2O_3)	24.1
Strontium oxide (SrO)	7.2
Nitrogen (N_2)	1.4
Carbon dioxide, water, etc. (CO_2,H_2O)	

[1]from Simpson and Woodley (1970)

The pyrotechnic flare was placed in a metallic cage, which was mounted in the wind tunnel. The flame temperature of the flare was estimated to be 2020°C. (Magnesium flame temperature is 5,072°C.) The chromel-alumel thermocouples that were used for the flame generator tests have a maximum temperature reading at 1,370°C. Therefore, we did not attempt to measure the flame temperature or its cooling rate. The character of the aerosols produced depends strongly on ventilation past the pyrotechnic during its ignition; therefore, for the pyrotechnic experiment we decreased the wind speed to 150 mph (66.6 m sec^{-1}) to simulate the terminal fall velocity of a flare. The aerosol collection procedures were the same as those for the flame generator tests. Because the combustion time for flares was approximately 1 min (50 to 55 sec), all sampling times were limited to 1 min after burning began, the flares left 35 g of coarse, gray residue in the mounting cage.

4.1. Size Distribution

Particles collected by the thermal precipitators are shown in figure 23. As the magnification increases—(a) 1600X; (b) 6500X; (c) 17400X; (d) 37400X—we can observe that each particle was actually a group of particles with some larger ones in the middle and numerous smaller ones encircling it. The particles seem to be formed from liquid droplets. However, the temperature of the flare is supposed to be higher than the boiling point of all the components in the flare, and the cooling rate was so rapid that the occurrence of molten AgI in the exhaust

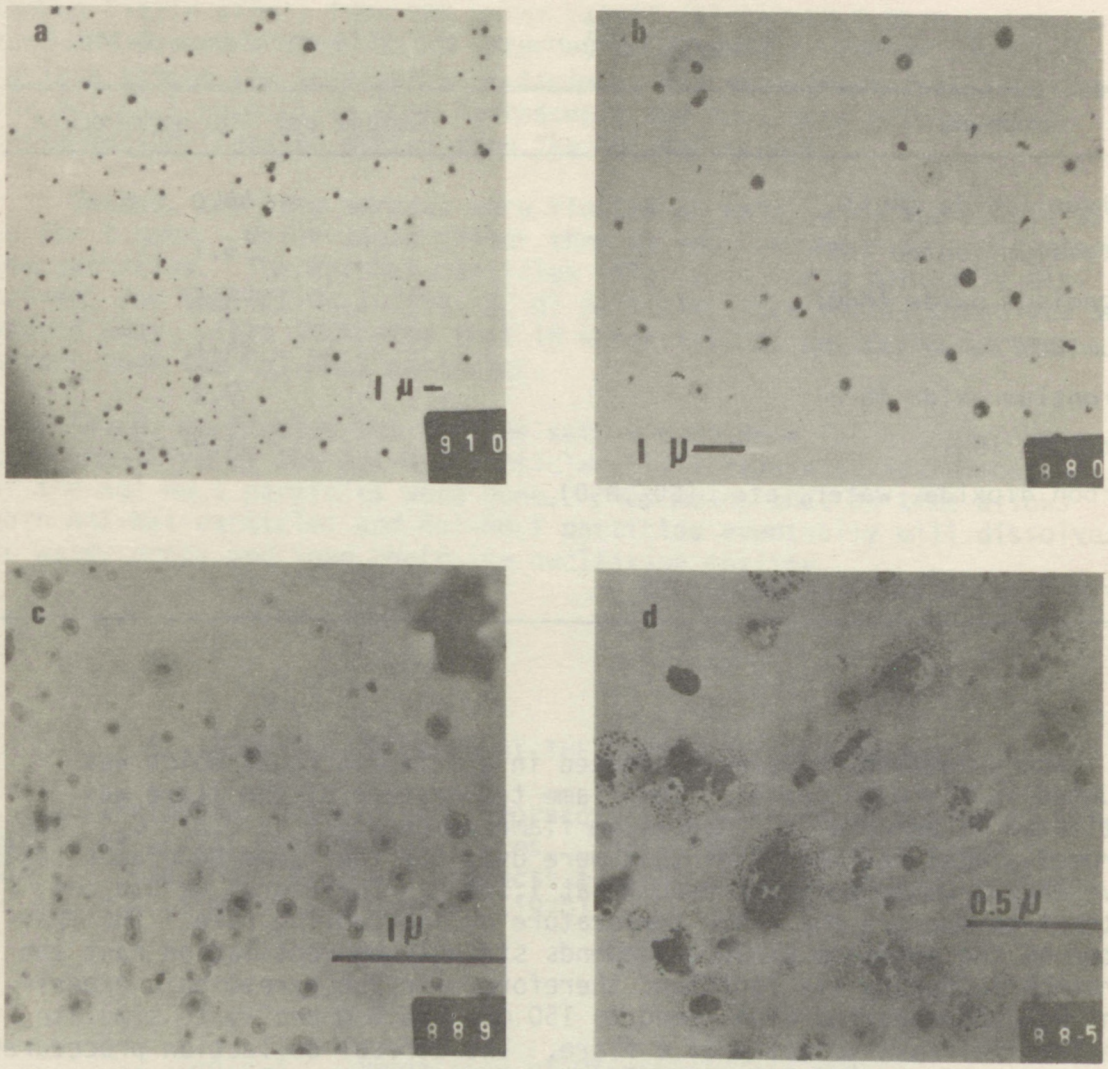

Figure 23. Electron micrographs of the aerosol produced by a pyrotechnic.

plume seems unlikely. The formation of condensed drops can be ruled out since here the solid phase forms first. In the humid air (>90 percent humidity) and reduced pressure (650 mm Hg) inside the wind tunnel, the generated particles acted as condensation nuclei to form water drops. The insoluble materials such as AgI, Al_2O_3, etc. remained solid inside the drops while the soluble materials, KI, SrO, AlI_3, etc. dissolved. After being collected by the sampler, the drops evaporated and left a residue of the soluble materials around the insoluble materials.

Determining the size distribution of the aerosols was difficult because of this complicated formation. If we assume the size of the ring was the actual size of the water drop we would have an unrealistically large measurement; if we counted all the fine particles around the ring, we would also get erroneous measurements. For simplicity, we measured only the insoluble particles, which were the dark portion inside the drops. The results of the size distribution are shown in figure 24; the median diameter is 0.09μ. The actual size of the original exhausted particles, which include the soluble components, should be slightly larger than our measurements show. For an accurate size determination, we should collect the samples on days having low humidity.

4.2 Chemical Analysis

We used X-ray energy spectrometry (XES) to determine the elemental composition of individual particles collected on the filters, as we did for the samples from the flame generators. From the analysis of 500 particles whose diameter was from 0.02μ to 10μ, we found only 25 percent of the particles were pure AgI (fig. 25); the majority (55 percent) were mixtures of Ag, I, Mg, Al, K, and Sr, which were the elements of the compounds in the flare. In addition, 15 percent of the particles were iodide mixture without silver and 5 percent were silver particles without iodine.

The use of silver iodate ($AgIO_3$) in a pyrotechnic requires complete thermal decomposition to liberate the Ag and I_2, which upon cooling recombine to form AgI. Evidently Ag and I_2 not only react to each other, but also mix with the other combustion products; 20 percent of the Ag and I did not exist in the same particles. Table 4 lists the quantities of the expected exhaust products; these are hypothetical values based on the thermodynamics of the flare's stoichiometric mixture. If these compounds were produced in the exhaust, they did not exist as individual particles. They were mixed or compounded with one another. The qualitative and quantitative analysis of individual particles would be very complicated problems because there were five or six compounds that passed through high heat and rapid cooling. Reactions such as evaporation, decomposition, gas phase reaction, and gas-solid transition took place in high ventilation airflow. Thus, the actual exhaust products could vary a great deal from the theoretical predictions. Because the flare did not burn completely, the metallic residues left by the flares contained mostly magnesium, aluminum, strontium, and silver (fig. 26), as determined by XES.

4.3. Hygroscopic Properties

When we collected the pyrotechnic aerorsol samples, we observed (fig. 23) that the particles collected moisture that condensed into water droplets, indicating they were very hygroscopic and could be

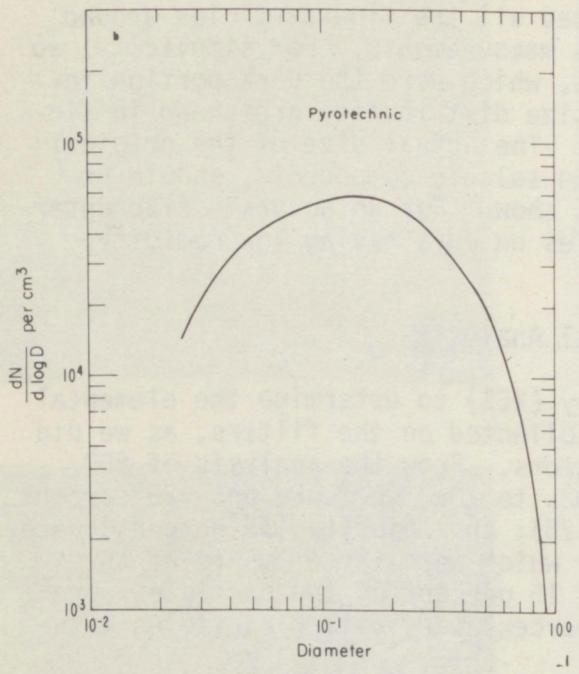

Figure 24. Size distribution of the pyrotechnic aerosol.

active condensation-freezing nuclei. A sample screen with pyrotechnic aerorol on it was floated on water sample side up for 15 min. The electron micrographs (fig. 27 a and b) show that the ring of fine particles disappeared and the larger particles inside remained. The same screen was soaked in water for 2 more hours. Surprisingly, some particles still remained (fig. 27c and d). This indicated that the pyrotechnic aerosol could survive in water for a long time and would be a good freezing nucleus. These insoluble particles were analyzed by XES and proved to be mainly AgI (70 percent). Aluminum was also found in 20 percent of the particles, presumably they were Al_2O_3. In addition, $CaSO_4$, SiO_2, Fe, etc. were also found in small amounts; undoubtedly they were ambient aerosols in the wind tunnel at Atlantic City (fig. 27 e and f).

When we studied the particles produced by a flame generator (sec. 2.5), we used the ratio between the Ag and I X-ray intensities to detect photodecomposition of the AgI particles. However, this method is unsuitable for examining the photodecomposition of pyrotechnic particles, because they were found as mixtures of multi-elements and their silver contents varied from 0 to 100 percent. We did not attempt to investigate the photostability of the pyrotechnic aerosol.

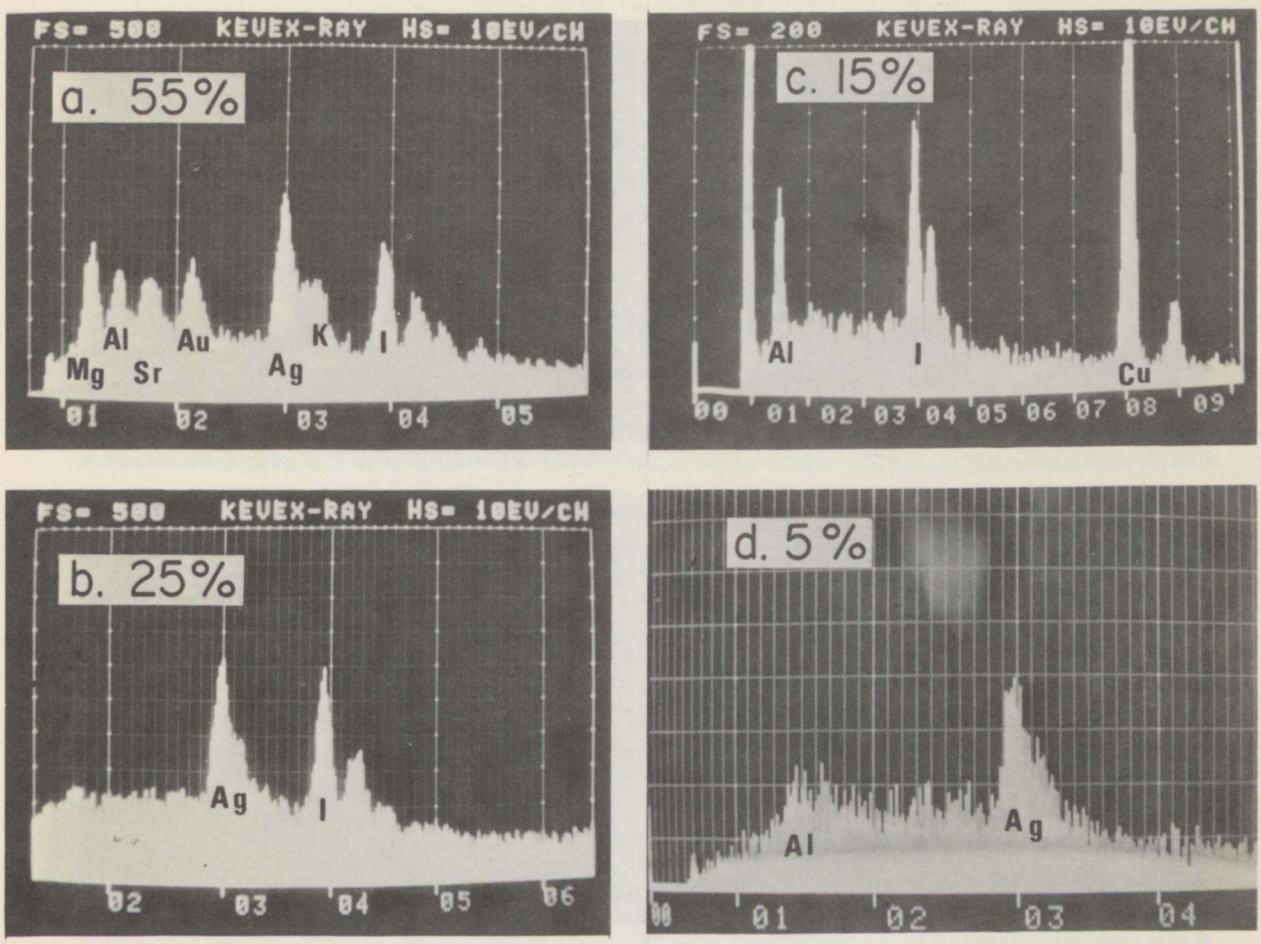

Figure 25. XES of the particles produced by a pyrotechnic.

5. AEROSOLS PRODUCED BY EVAPORATING OF SOLID SALTS IN A FLAME GENERATOR

We tested the two existing types of AgI aerosol generators, the phyrotechnic and the flame generator, and found that both methods have apparent disadvantages. The particles produced by the pyrotechnic were relatively large and chemically poorly defined. They would be good condensation-freezing nuclei but poor contact nuclei. The particles produced by the flame generators were small and also mixed with hygroscopic additives such as KI, NaI, or NH_4I. Consequently, they will easily dissolve in cloud droplets and, thus, they have a limited lifetime as ice nuclei.

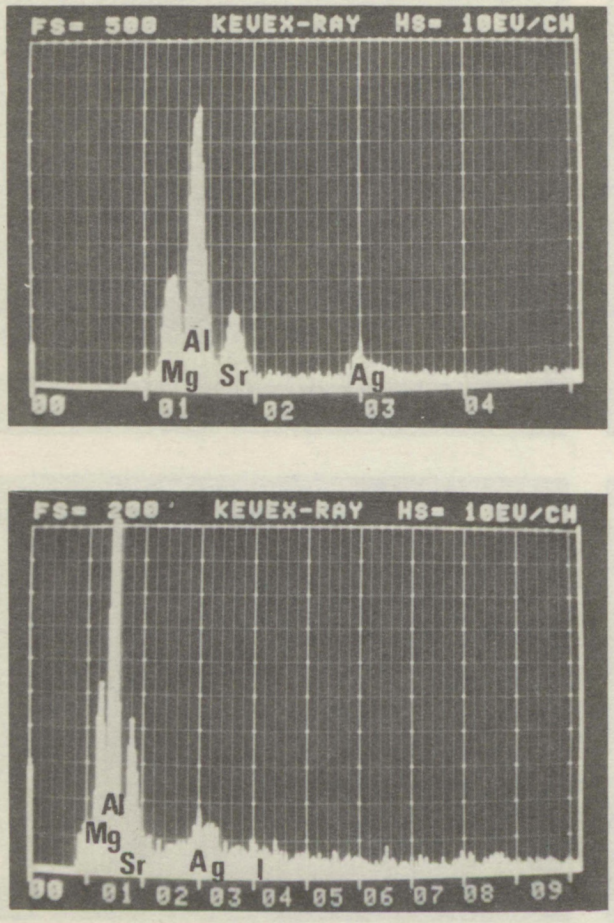

Figure 26. XES of the residue of a combusted pyrotechnic.

Because of these problems, we developed a new generating method to test whether we could control the aerosols' size distribution, chemical composition, and physical properties. Patten et al. (1971) designed a new flame generator system (fig. 28). Solid salts (s) are injected directly into the combusion chamber (c); gasoline, acetone, or other fuels (f) can be used for ignition. Solid seeding materials can be injected from 0.5 to 360 g min^{-1} by regulating the injection pressure (P). Evaporation takes place in the combusion chamber and recondensation at a supersaturated state occurs in the exhaust plume.

The experiment was carried out in the FAA wind tunnel at a wind speed 200 mph (88.8 m sec^{-1}). Three different solids were burned in the modified flame generator: pure AgI; AgI and NaI mixed in equal amounts; and AgI and NaI mixed in a 1 to 2 ratio. We collected the aerosols and analyzed them in the same way as for the previous experiments.

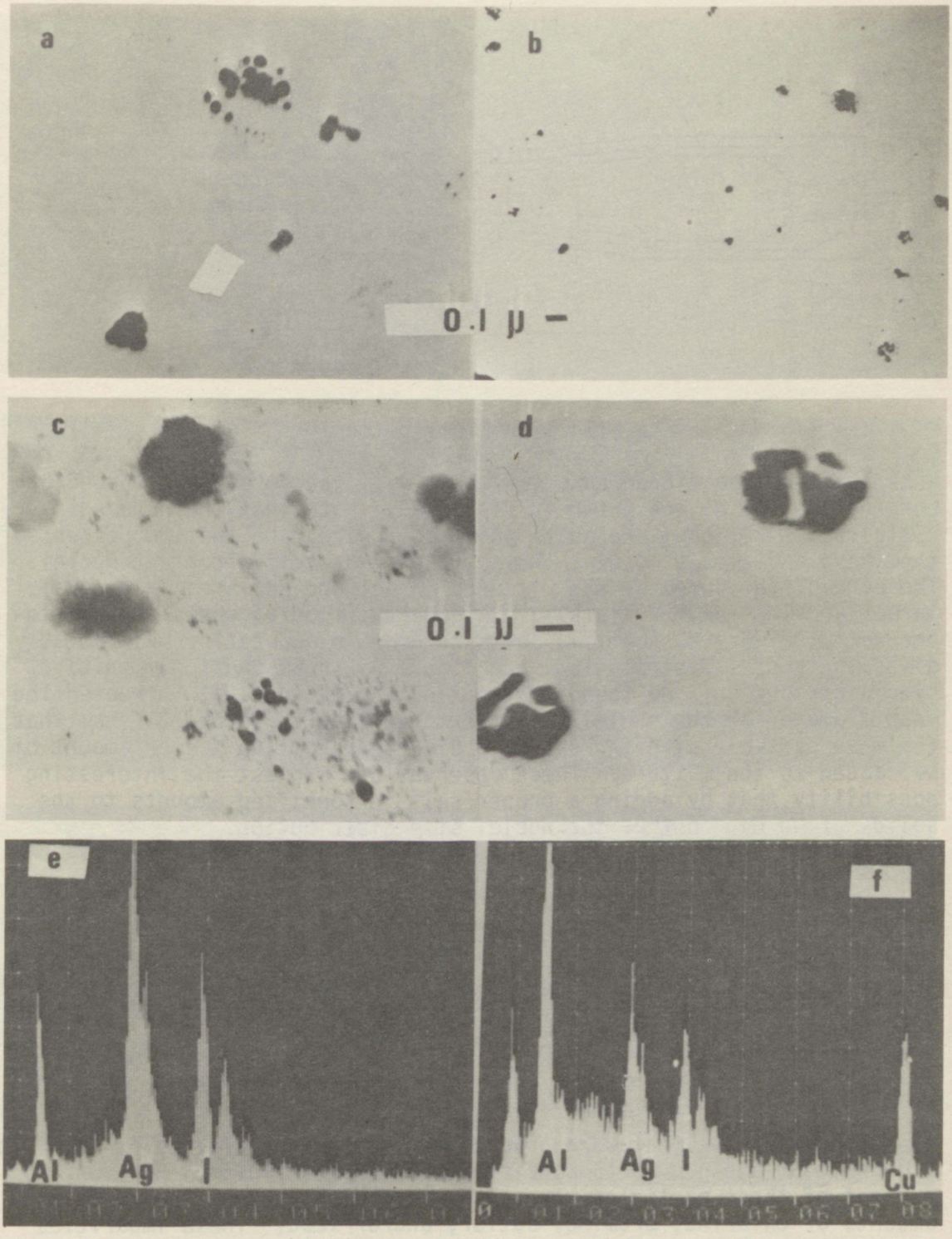

Figure 27. Pyrotechnic particles: (a and b) contacted with water for 15 minutes; (c and d) soaked in water for 2 hours; (e and f) XES of the water treated particles.

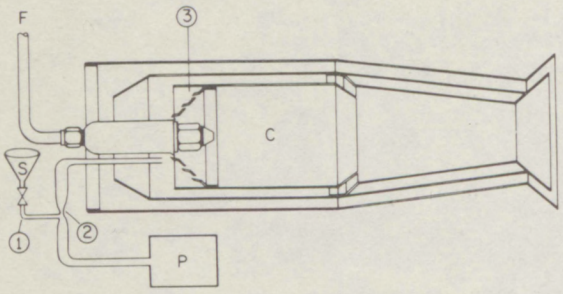

Figure 28. Diagram of the modified flame generator for combusting solid salts.

5.1 Size Distribution

The electron micrographs (197,400 X) of the aerosols produced by burning the solids are shown in figure 29. Note that the pure AgI particles (fig. 29, top) are quite uniform in size, and that 90 percent of them have a diameter $<0.02\mu$; they can serve as active contact nuclei. The aerosols produced by the mixtures of AgI and NaI are, in general, larger and less uniform in size. Figure 29 (middle) shows the one-to-one ratio; figure 29 (bottom) shows the one-to-two ratio. Figure 30 gives their size distribution, and figure 31 shows their cummunitive size distribution. We found that mixing the AgI and NaI increased the mean diameter of the nuclei. Furthermore, figures 30 and 31 show that the mean particle size increases in direct proportion to the amount of NaI added to the mixture. These observations suggest the interesting possibility that by adding a proper salt in specified amounts to the solid AgI we can control the nuclei size distribution.

5.2 Chemical Analysis

Elemental analysis of the individual particles was determined by the XES, whose sensitivity is limited to a particle diameter $\geq 2 \times 10^{-2}\mu$. Therefore, only the large particles can be analyzed.

5.2.1 *Pure AgI*

The particles that were produced by injecting pure, solid AgI into a gasoline flame proved to consist of silver and iodine. However, 30 percent of these particles were also mixed with various, but small, amounts of chlorine, bromine, sulfur, and/or lead. These impurities were undoubtedly from the gasoline exhaust.

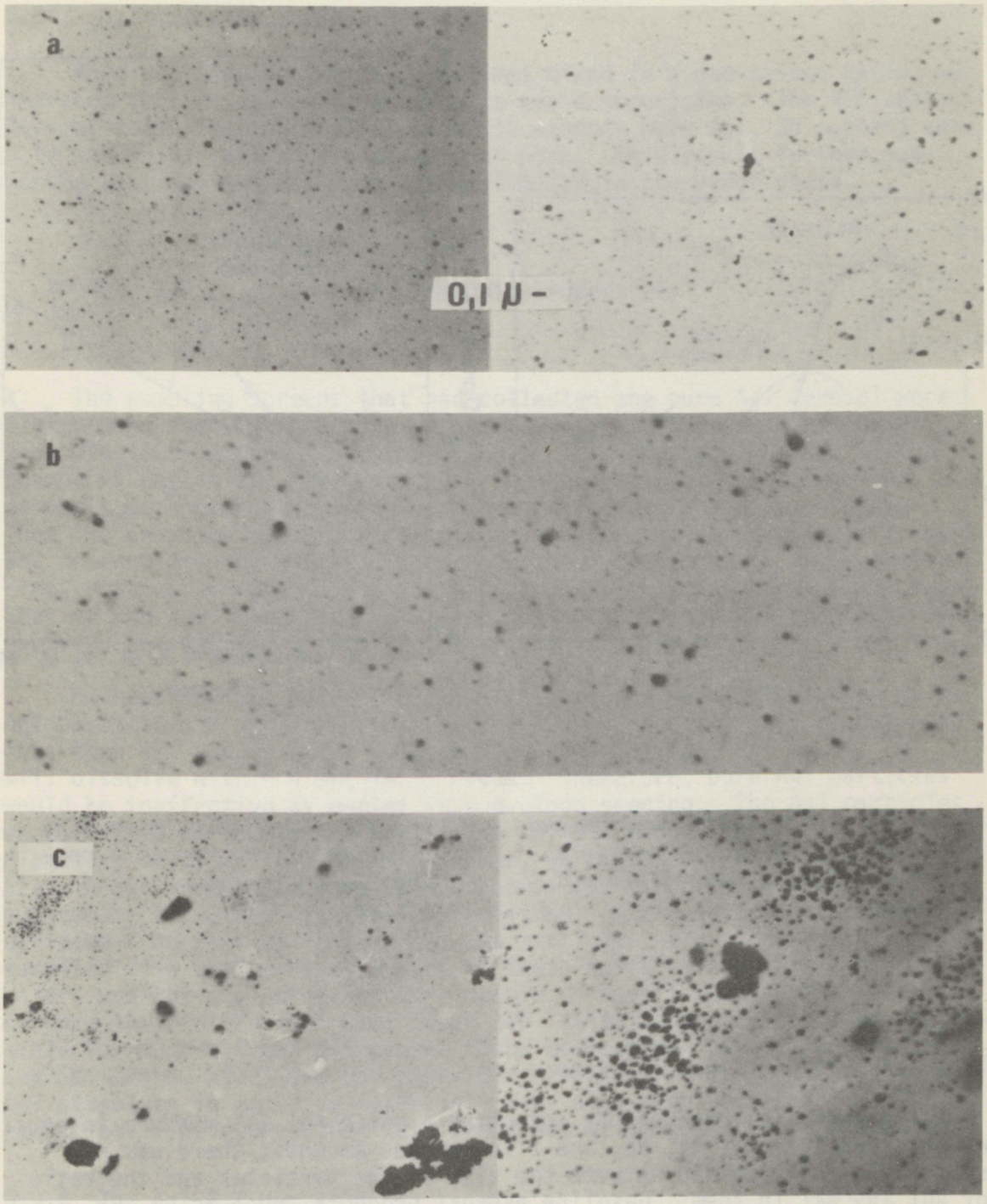

Figure 29. Electron micrographs of the aerosols produced by injection of solids into the generator: (a) pure AgI; (b) AgI and NaI, 1 to 1 weight ratio; (c) AgI and NaI, 1 to 2 weight ratio.

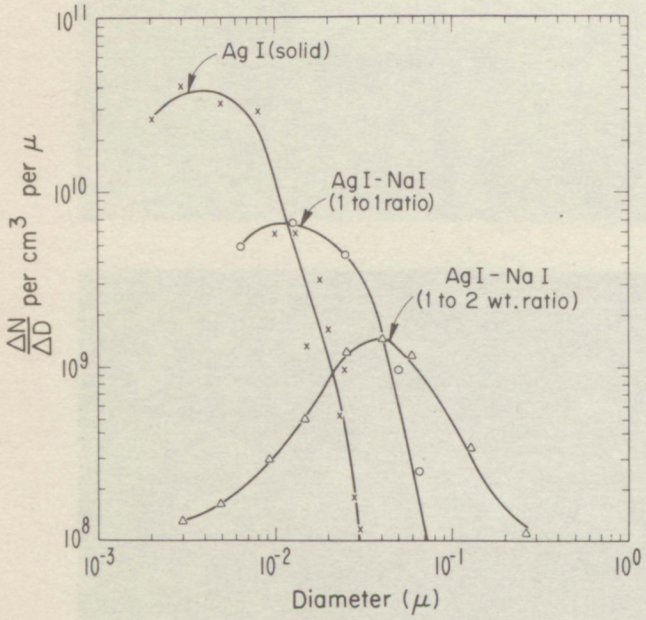

Figure 30. Size distributions and concentrations of the aerosols produced by injection of solid iodides.

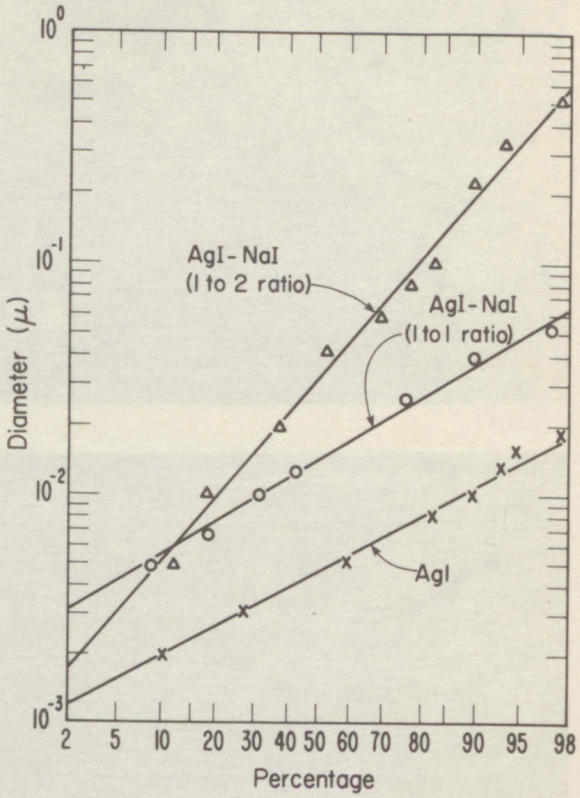

Figure 31. Cumulative size distribution of the aerosols produced by injection of solid iodides.

5.2.2 *AgI-NaI in Equal Portions*

The particles produced by injecting a solid AgI-NaI mixture in equal weights consisted of Ag, Na, and I in various amounts; there was no systematic relationship between the size of the particles and the ratio of AgI and NaI in them. Gasoline exhaust products, such as Cl, Br, S, and Pb, also appeared in different quantities. The explanation for the formation of these randomly mixed particles is that AgI and NaI were not mixed and evaporated homogeneously in the flame; the particles formed by the vapor-solid transition thus had various proportions of AgI and NaI.

5.2.3 *AgI-NaI in a One-to-Two Ratio*

When we injected the solid AgI-NaI mixed in a one-to-two ratio, we replaced the gasoline with acetone to avoid impurities. The XES analysis of individual particles showed 15 percent were AgI, 30 percent were NaI, and 55 percent were a mixture of both. This result further suggested that AgI and NaI were not well-mixed in the vapor phase.

5.3 Hygroscopic Properties

5.3.1 *Pure AgI*

The sampling screens that had collected the pure AgI aerosol were floated on water, sample side up, for 30 min and then examined by a transmission electron microscope (TEM). This treatment caused little change in particles' size, shape, or concentration, indicating the aerosols were hydrophobic and unable to serve as condensation nuclei. Then the sampling screens were soaked in water for an additional 2 hours and re-examined with a TEM. Figure 32 shows that most of these particles, remained on the film with spots and stain around them. This means that on the particle-water interface, dissociation of AgI had occurred; however, the diffusion into the water was incomplete.

Mathews and St. Amand (1972) calculated the rate of solution of an AgI particle and predicted that nuclei <0.01μ (radius) will dissolve in less than 400 sec in water drops having radii of 40μ, and 0.001μ AgI will dissolve within 4 sec in 5μ drops. Therefore, pure AgI particles would be ineffective as nuclei in sub-cloud seeding. The AgI particles we collected on the screen have sizes in this range (90 percent with diameters of 0.02μ to 0.002μ. However, we found they were able to survive in bulk water for more than 2 hours; our experimental results apparently disagreed with their prediction. Although our experiment deviated from reality in that (a) the particles were attached to the sampling film that protected part of their surface from interacting with water, and (b) the particles were unable to move freely in the water to enhance their diffusion rate; these two limitations should not be responsible for such a great difference found between the prediction (Mathews and St. Amand, 1972) and our experimental results. The rate that pure AgI dissolves in water is definitely very slow even for these small particles. Therefore, they have great potential for sub-cloud seeding.

5.3.2 *The AgI-NaI Mixtures*

When we used a large magnification to examine the particles from the AgI-NaI mixture in one-to-two ratio (fig. 33, 47,000 X), we observed that some were actually a group of small particles forming a ring around

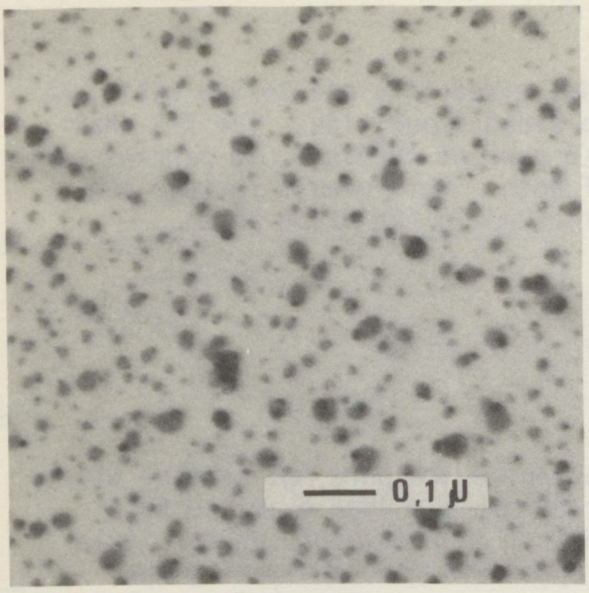

Figure 32. Pure AgI aerosol after being treated in water for 2 hours.

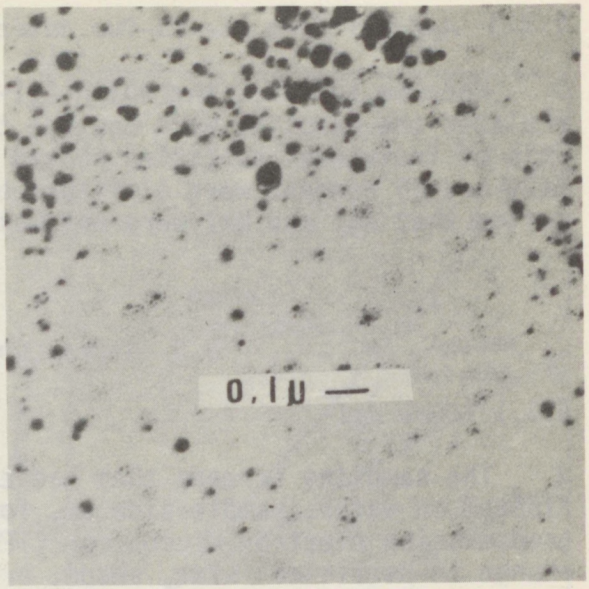

Figure 33. Electron micrographs of the aerosol produced by injection of AgI and NaI at 1 to 2 weight ratio.

wind tunnel and formed liquid drops that contained soluble NaI and insoluble AgI. After drying, the soluble portion formed a residue around the insoluble particle. Therefore, the aerosol generated with the AgI-NaI mixtures were very hygroscopic.

Electron-microscopic screens with samples of particles which were generated by combustion of AgI and NaI in one-to-one mixing ratio or one-to-two ratio were floated on water for 30 min. Almost all the particles dissolved. These results suggested that the addition of solid NaI to the AgI produced particles with not only increased geometric mean sizes but also with increased hygroscopic character. Therefore, these mixed aerosols would be active condensation-freezing nuclei.

6. ICE NUCLEATION EFFECTIVENESS OF THE AgI AEROSOLS

This investigation of AgI aerosols produced by the different methods was improve our understanding of the relationship between the aerosols' properties and their ice nucleation effectiveness. Once we know these effects we can then select or develop a method to generate the AgI aerosols that have the highest ice nucleation activity. There are many

techniques for measuring nucleation ability. Because the aerosol samples that we brought back from the wind tunnel experiments were collected on membrane filters, we were limited to analyzing their activity with a membrane ice nucleus counter.

Langer and Rogers (1975) at NCAR constructed a new ice crystal developing unit, where ice nuclei collected on a membrane filter are activated at a controlled temperature and humidity to produce ice crystals. This unit is a modification of the conventional thermal gradient chamber (Gagin and Arroyo, 1969; Stevenson, 1968), but it has a flow system that provides a continuous source of water vapor from a humidifier. Two kinds of humidifiers were used. One was a "condensation development humidifier"; clean air is saturated at the vapor pressure of the ice which is cooled to a well-controlled temperature. By regulating the temperature difference between the sample on the membrane filter and the ice in the humidifier, we can control the degree of saturation with respect to ice or water on the sample's surface. The other humidifier is called a "cloud development humidifier." By expansion of moist air, cloud droplets form and are added to the airflow over the sample. The ice crystals grown on the membrane filter at these controlled conditions are counted with an optical microscope.

All the ice nucleus measurements were conducted by Langer and Rogers at NCAR. Table 5 shows the ice nucleus concentration of AgI

Table 5. Pyrotechnic Ice Nucleus Concentration (nuclei ℓ^{-1}) on Membrane Filters.

Filter	Sampling Rate (ℓ min^{-1})	-6°C		-8°C		-16°C	
		RH 103%	Cloud	RH 100%	Cloud	RH 95%	Cloud
Nucleopore							
0.4 μ	0.5	16	144	-	-	-	-
	5.0	0	0	-	-	-	-
Sartorius							
0.1 μ	0.5	32	80	192	0	60	3.4×10^5
	5.0	6.3	6.3	23	3.5×10^3	51	5.5×10^4
Sartorius							
0.2 μ	0.5	80	96	80	2×10^3	0	2.5×10^5
	5.0	11	2.4	0	100	32	2.6×10^4
Aquapel							
0.2 μ	0.5	0	48	20	0	20	1.8×10^5
	5.0	248	748	19	1×10^3	84	8×10^4
Millipore							
0.45 μ	0.5	0	0	48	496	500	6.8×10^4
		0	32	-	-	1.2×10^3	2.1×10^5
	5.0	88	472	13	2.8×10^3	390	3.2×10^4
		0	112	-	850	260	too many

RH= relative humidity

aerosol produced by pyrotechnics. As we can see, the ice nucleus count not only depends on the filters' materials and pore sizes, but also depends on the sampling flow rate. Therefore, for comparison, we used the same type of filter, identical sampling conditions, and measured the ice nuclei simultaneously by placing the filters side by side in the membrane ice nucleus counter. We used 0.1μ Millipore filter to collect the aerosols produced by a flame generator; both AgI-NaI and AgI-NH_4I aerosols were sampled at the two flow rates, 12 ℓ min^{-1} and 8 ℓ min^{-1}. The ice nucleus concentration on these two sets of filters could then be compared realistically.

Aerosols produced by the pyrotechnic were collected on many different types of filters, but none on the 0.1μ Millipore filter. The pyrotechnic sample that was most similar to the flame generator sample was collected at 5 ℓ min^{-1} flow rate on a 0.1μ Sartorius filter. We were obliged to use its ice nucleus concentration data for the comparison with the flame generator samples. The results are listed in Table 6 and figure 34. The data points of the AgI-NaI and the AgI-NH_4I in figure 34 are the average values of the two runs (at 12 ℓ min^{-1} and 8 ℓ min^{-1}).

Table 6. Ice Nucleation Activities (nuclei ℓ$^{-1}$) of AgI Aerosols.

Sample	Sampling Rate (ℓ min^{-1})	°C at RH 95%				°C at RH 103%				°C in Cloud			
		-6	-8	-12	-16	-6	-8	-12	-16	-6	-8	-12	-16
AgI-NaI on 0.1μ Millipore	12	0	0	1.3	2.3	0	17	-	137	0	1×10^3	3×10^3	2.7×10^4
	8	0	0	43	8.5	0	44	-	109	2	7.5×10^3	3.4×10^3	5.3×10^4
AgI-NH I on 0.1μ Millipore	12	0	0	127	30	0.3	80	-	175	0.3	1×10^4	too many	4.0×10^4
	8	0	0	78	25	0.5	101	-	220	1	1×10^4	4.7×10^3	3.4×10^4
Pyrotechnic on 0.1μ Sartarius	5	0	0	52	3	6.3	61	-	240	6.3	1.3×10^4	5.5×10^4	1.1×10^5

RH = relative humidity

For testing the aerosols ice nucleation effectiveness with a membrane ice nucleus counter, we regulated the humidity to simulate three different nucleation conditions: sublimation, condensation-freezing, and contact.

When the humidity is regulated to 95 percent of water saturation, but at ice supersaturation with the condensation development humidifier, we should obtain the ice nucleus count as sublimation ice nuclei. Figure 34 and Table 6 show no ice nucleus was observed at temperatures

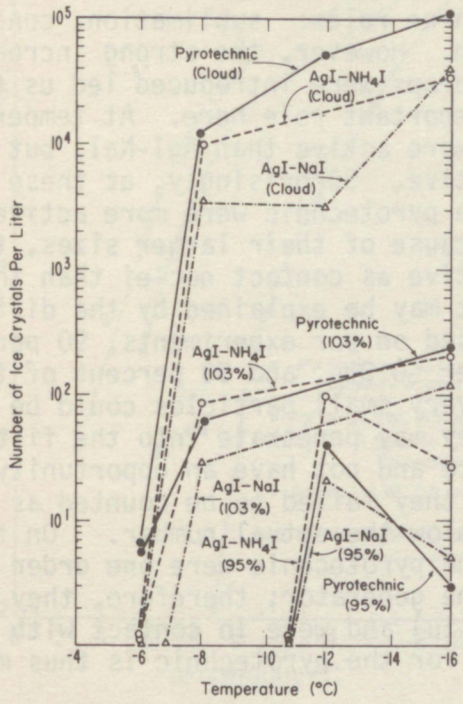

Figure 34. Effectiveness of ice nuclei produced by the different methods determined by membrane filter ice nucleus counter.

warmer than -8°C. At -12°C and -16°C, nuclei produced by all three methods — pyrotechnic, AgI-NaI, and AgI-NH_4I — were starting to be active as sublimation nuclei. However, their activities remained very low.

When the humidity is adjusted to 103 percent, nuclei will act as condensation freezing nuclei. At -6°C, the particles produced by the AgI-NH_4I and by the pyrotechnic began to be active, but not the AgI-NaI particles. At -8°C the AgI-NH_4I was the most active, the pyrotechnic and second, and the AgI-NaI the least active as condensation freezing nuclei. At -16°C, the AgI-NH_4I and the pyrotechnic still yielded more ice crystals than the AgI-NaI. However, the difference had narrowed to fractions. These results may be explained by the composition and properties of the aerosols. The surface of the AgI-NaI particles was found to be hydrophoic AgI, while the AgI-NH_4I and pyrotechnic products were enriched with hydrophilic additives. Therefore, of the three products, the AgI-NaI would be the poorest condensation-freezing ice nucleus.

When the "cloud development" humidifier was used, cloud droplets were introduced on the sample filters to cause ice nucleation. The nuclei on the filters can act in all three roles: sublimation, condensation-freezing, and contact nucleation. However, the strong increase in the ice crystal counts after cloud drops were introduced led us to believe contact nucleation played an important role here. At temperatures warmer than -12°C, AgI-NH_4I was more active than AgI-NaI, but at -16°C they both were almost equally active. Surprisingly, at these cloud conditions, the aerosols from the pyrotechnic were more active than those of the flame generator. Because of their larger sizes, the pyrotechnic aerosols should be less active as contact nuclei than those of the flame generator too. The result may be explained by the difficiency of the measuring technique. Based on our experiments, 90 percent of the AgI-NH_4I particles had a diameter $\leq 0.01\mu$, and 90 percent of the AgI-NaI particles were $\leq 0.02\mu$. These very small particles could be most active as contact nuclei. However, they may penetrate into the filter pores (0.1μ) or coagulate on its surface and not have an opportunity to contact the water droplets; therefore, they failed to be counted as ice nuclei causing the measurement to be below the actual number. On the other hand, the aerosols produced by the pyrotechnic were one order of magnitude larger than those of the flame generator; therefore, they stayed on the surface of the filter (0.1μ) and were in contact with water droplets. The ice nucleus count for the pyrotechnic is thus more accurate.

Previously, Patten (1971) tested the nucleation activities of AgI-NaI and AgI-NH_4I aerosols that were produced by the same generator in the isothermal cloud chamber at Colorado State University. Simpson (1970) reported the nucleation effectiveness of the pyrotechnic aerosols that were measured in the same cloud chamber. Their results, summarized in figure 35, agreed with David and Steele's (1968) experimental conclusion that at temperatures warmer than -12°C, the aerosol produced by a steady-state flame generator is, in general, more effective than the aerosol of a pyrotechnic, but the difference between their effectiveness decreases at lower temperatures. Nevertheless, because all of these experiments were done on the ground and were not simulated in-flight conditions, they are subject to the criticism that they may vary from actual conditions present during seeding.

Allee et al. (1972) performed a dynamic calibration on a flame generator in actual flight. They found that the AgI aerosol produced in flight was in general less concentrated than that derived in the cloud chamber, and that the AgI-NH_4I system performed better by a factor of two than the AgI-NaI system, as indicated in figure 35.

In conclusion the available data on the effectiveness of aerosols produced by different methods are either inadequate or unsuitable to compare their ice nucleation effectiveness. At present, there is no method for segregating the activity of a certain type aerosol, as it

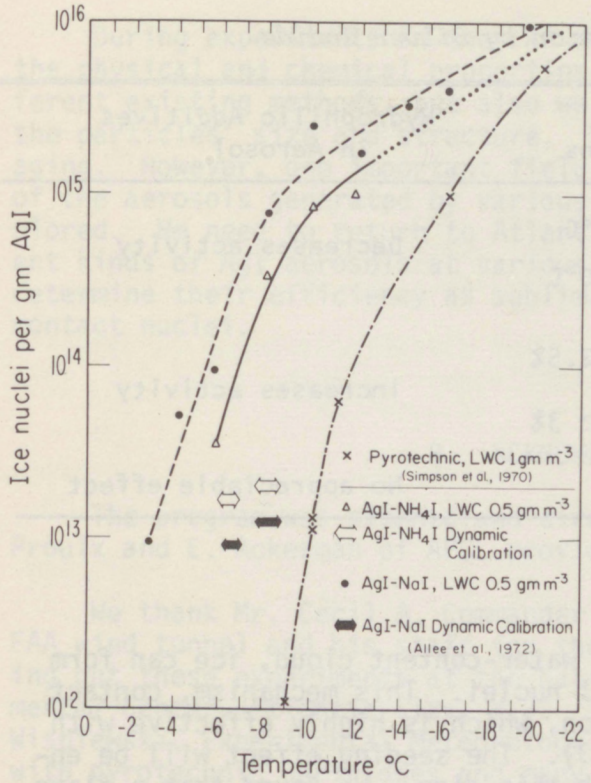

Figure 35. Effectiveness of ice nuclei produced by the different methods determined in CSU cloud chamber and the dynamic calibration.

acts as a sublimation nuclei, a condensation-freezing nuclei, or a contact nuclei. Since determining ice nucleation effectiveness of AgI aerosols is one of the most important goals of our investigation, we must develop more precise methods to measure and to segregate the ice nucleation abilities of various AgI aerosols at different simulated airborne cloud seeding conditions.

7. CONCLUSIONS

Because silver iodide is an expensive chemical and its effects on humans, animals, and vegetation are unknown, its massive and prolonged use as a cloud seeding agent often causes concern. Therefore, we should use AgI in the most sparing but effective way. One fundamental approach is to understand the role AgI plays in the three ice nucleation mechanisms: sublimation, condensation-freezing, and contact nucleation. To occur, each mechanism requires AgI nuclei with specific chemical and physical properties that complement the particular cloud conditions. Table 7 lists the characteristics of AgI aerosols as they affect these mechanisms.

For an effective cloud seeding operation, we should first know the meteorological conditions, then we can select an appropriate ice nucleation mechanism, and deliver the AgI nuclei having the properties required for activating that mechanism.

Table 7. Ice Nucleation by Silver Iodide

Mode of Ice Nucleation	Effective Size/Conditions	Hydrophilic Additives in Aerosol
Sublimation	r > 0.1μ at -10°C r > 0.02μ at -20°C	Decreases activity
Condensation-Freezing	r > 1μ at SS ≥ 2.5% r > 0.1μ at SS ≥ 3%	Increases activity
Contact	r < 0.02μ	No appreciable effect

SS = supersaturation

When we use AgI to seed a high water-content cloud, ice can form by cloud droplets contacting the AgI nuclei. This mechanism, contact nucleation, is due to Brownian motion, which is highly effective with a particle radius ≤0.02μ (Junge 1963). The seeding effect will be enhanced by delivering AgI nuclei with this size. We found that a flame generator using an AgI-NH_4I acetone solution, an AgI-NaI acetone solution, or pure, solid AgI produces particles with a radius ≤0.02μ, which are desirable for contact nucleation.

When we deliver AgI nuclei below a cloud base, hoping an up-draft will carry them into the cloud, ice crystals will form through condensation-freezing nucleation. A hygroscopic salt mixed with the AgI would enhance condensation to form water droplets. However, the particles should be large enough (e.g., have a radius of 1μ at a water supersaturation of 2.5 percent) to avoid being completely dissolved into the droplets and lose their ice nucleation ability. For this application, we propose using a pyrotechnic or a flame generator burning a mixture of solid AgI and NaI to produce condensation-freezing nuclei.

When we seed clouds to exploit the sublimation nucleation process, the two-dimensional epitaxial phenomenon plays an important role; the surface of the host nucleus requires a minimal misfit with the corresponding ice surface. Thus, impure AgI particles are undesirable. In addition, Fletcher (1966) stated that AgI acts as a sublimation nucleus at -10°C only if its radius ≥0.1μ and at -20°C only if its radius >0.02μ. Therefore, we should use pure, large AgI particles for stimulating sublimation nucleation. We suggest that aerosols produced by a flame generator burning pure, solid AgI would be suitable for this purpose.

During experiments in the FAA wind tunnel we not only investigated the physical and chemical properties of the AgI nuclei generated by different existing methods, but also we developed new methods to control the particles' size and structure. The preliminary results are encouraging. However, one important field, the ice nucleation effectiveness of the aerosols generated by various methods, has not been well explored. We need to return to Atlantic City, N. J., to test the different kinds of AgI aerosols at various simulated cloud conditions, and to determine their efficiency as sublimation, condensation-freezing, and contact nuclei.

8. ACKNOWLEDGMENTS

The program was planned and directed by Dr. H. K. Weickmann. R. A. Proulx and E. Ackerman of APCL provided technical assistance.

We thank Mr. Cecil A. Commander for his cooperation in using the FAA wind tunnel and his staff for their technical assistance in carrying out these experiments at the National Aviation Facilities Experimental Center, Atlantic City, N.J. Dr. R. I. Sax and Mr. Joseph Wisniewski, Experimental Meteorology Laboratory, ERL, NOAA provided us with pyrotechnic cartridges and many valuable suggestions. We are also grateful to Mr. G. Langer and Mr. James Rodgers of NCAR's National Hail Research Experiment for measuring ice nuclei on the membrane filters.

9. REFERENCES

Allee, P. A., B. T. Patten, and E. W. Barrett, 1972: The dynamic calibration of an airborne ice nuclei generator. *J. Rech. Atmos.* 6, 29-40.

Burley, G., 1963: Polymorphism of silver iodide. *Amer. Mineral.* 48, 1266-1276.

Davis, C. I. and R. L. Steele, 1968: Performance characteristics of various artificial ice nuclei sources. *J. Appl. Meteor.* 7, 667-673.

Davis, B. L., L. R. Johnson, and F. J. Moeng, 1973: Particle size of cloud seeding serosols obtained by wide-angle and small-angle X-ray scattering. *Nerelco Reporter*, 20(2), 15-20.

Eyre, D., 1974: Wind tunnel tests of an airborne iso-kinetic ice crystal decelerator. NOAA Tech. Memo ERL APCL-18.

Fletcher, H. H., 1959: Entropy effect in ice crystal nucleation. *J. Chem. Phys.*, 30, 1476-1482.

Fletcher, N. H., 1966: *The Physics of Rain Clouds*, Cambridge University Press, N. Y., 386 pp.

Frank, E. R., K. R. Spurny, D. C. Sheesley, and J. P. Lodge, Jr., 1970: The use of nuclepore filter in light and electron microscopy of aerosols, *J. du Microscopie*, 9, 735-740.

Gagin, A., and M. Arroya, 1969: A thermal diffusion chamber for the measurement of ice nuclei concentrations. *J. Rech. Atmos.*, 4, 115-122.

Isono, K. and Y. Tshizaka, 1968: On ice nucleating properties of different faces of silver iodide crystals. *J. Rech. Atmos.*, 3, 139-140.

Junge, C. E., 1963: *Air Chemistry and Radioactivity*, International Geophysics Series, 4, Academic Press, N. Y., 382 pp.

Langer, G. and J. Rodgers, 1975: An experimental study of the detection of ice nuclei on membrane filter and other substrata. To be published *J. Appl. Meteor.*

Mason, B. J. and J. Hallett, 1956: Artificial ice-forming nuclei. *Nature*, 177, 681-683.

Mathews, L. A., and P. St. Amand, 1972: The contribution of interfacial kinetics and of diffusion to the rate of solution of silver iodide particles and its effect on nucleation. *3rd Conf. on Weather Modification*, Rapid City, S.D., 1-4 (Am. Meteor. Soc.).

Mossop, S. C., and C. Tuck-Lee, 1968: The composition and size distribution of aerosols produced by burning solution of AgI and NaI in acetone. *J. Appl. Meteor.*, 1, 234-240.

Patten, B., T., 1972: Information and data sheet for Patten Mark Series Generators, On file at RFF, NOAA, Miamia, Florida.

Patten, B. T., J. D. McFadden, and H. A. Friedman, 1971: Airborne cloud seeding system developed and utilized by Research Flight Facility. *Proc. Int. Conf. on Weather Modification*, Canberra, Australia, p. 358 (Australia Academy of Science and Am. Meteor. Soc.).

Pena, R. G. and E. A. Caimi, 1967: Hygroscopicity and chemical composition of silver iodide smoke used in cloud seeding experiments. *J. Atmos. Sci.*, 24, 383-386.

Reynolds, S. E., W. Hume, and M. McWhirter, 1951: Effects of sunlight and ammonia on the action of silver-iodide particles as sublimation nuclei. *Bull. Am. Meteor. Sci.*, 33, 26-31.

Sax, N. I., 1963: *Dangerous Properties of Industrial Materials.* 2nd Ed., Reinhold, N. Y., 1343 pp.

Simpson, J. and W. L. Woodley, 1970: An airborne pyrotechnic cloud seeding system and its use. *J. Appl. Meteor.*, 9, 109-122.

Stevenson, M., 1968: An improved Millipore filter technique for measuring the concentration of freezing nuclei in the atmosphere. *Quart. J. Roy. Meteor. Soc.*, 94, 35-43.

Vonnegut, B., 1949: Nucleation of supercooled water clouds by silver iodide smoke. *Chem. Rev.*, 44, 277-289.

Watson, H. H., 1953: Errors due to anisokinetic sampling of aerosols. *Report of Symposium V, Aerosols*, 31-44. Army Chemical Center, Aberdeen Proving Ground, Md.

Weickmann, H. K., 1973: The Modification of Great Lake Winter Storms. *NOAA Tech. Rept., ERL-265-APCL 26* (GPO, D.C.), 103 pp.

☆U. S. GOVERNMENT PRINTING OFFICE 1975 - 677-347/1209 REG. 8

ENVIRONMENTAL RESEARCH LABORATORIES

The mission of the Environmental Reasearch Laboratories is to study the oceans, inland waters, the lower and upper atmosphere, the space environment, and the earth, in search of the understanding needed to provide more useful services in improving man's prospects for survival as influenced by the physical environment. Laboratories contributing to these studies are:

Atlantic Oceanographic and Meteorological Laboratories (AOML): Geology and geophysics of ocean basins and borders, oceanic processes, sea-air interactions and remote sensing of ocean processes and characteristics (Miami, Florida).

Pacific Marine Environmental Laboratory (PMEL): Environmental processes with emphasis on monitoring and predicting the effects of man's activities on estuarine, coastal, and near-shore marine processes (Seattle, Washington).

Great Lakes Environmental Research Laboratory (GLERL): Physical, chemical, and biological, limnology, lake-air interactions, lake hydrology, lake level forecasting, and lake ice studies (Ann Arbor, Michigan).

Atmospheric Physics and Chemistry Laboratory (APCL): Processes of cloud and preciptation physics; chemical composition and nucleating substances in the lower atmosphere; and laboratory and field experiments toward developing feasible methods of weather modification.

Air Resources Laboratories (ARL): Diffusion, transport, and dissipation of atmospheric contaminants; development of methods for prediction and control of atmospheric pollution; geophysical monitoring for climatic change (Silver Spring, Maryland).

Geophysical Fluid Dynamics Laboratory (GFDL): Dynamics and physics of geophysical fluid systems; development of a theoretical basis, through mathematical modeling and computer simulation, for the behavior and properties of the atmosphere and the oceans (Princeton, New Jersey).

National Severe Storms Laboratory (NSSL): Tornadoes, squall lines, thunderstorms, and other severe local convective phenomena directed toward improved methods of prediction and detection (Norman, Oklahoma).

Space Environment Laboratory (SEL): Solar-terrestrial physics, service and technique development in the areas of environmental monitoring and forecasting.

Aeronomy Laboratory (AL): Theoretical, laboratory, rocket, and satellite studies of the physical and chemical processes controlling the ionosphere and exosphere of the earth and other planets, and of the dynamics of their interactions with high-altitude meteorology.

Wave Propagation Laboratory (WPL): Development of new methods for remote sensing of the geophysical environment with special emphasis on optical, microwave and acoustic sensing systems.

Marine EcoSystem Analysis Program Office (MESA): Plans and directs interdisciplinary analyses of the physical, chemical, geological, and biological characteristics of selected coastal regions to assess the potential effects of ocean dumping, municipal and industrial waste discharges, oil pollution, or other activity which may have environmental impact.

Weather Modification Program Office (WMPO): Plans and directs ERL weather modification research activities in precipitation enhancement and severe storms mitigation and operates ERL's research aircraft.

NATIONAL OCEANIC AND ATMOSPHERIC ADMINISTRATION
BOULDER, COLORADO 80302

USCOMM - ERL